Global and Planetary Change 211 (2022) 103786

Contents lists available at ScienceDirect

Global and Planetary Change

journal homepage: www.elsevier.com/locate/gloplacha

# Key traits of living fossil *Ginkgo biloba* are highly variable but not influenced by climate – Implications for palaeo-$pCO_2$ reconstructions and climate sensitivity

M. Steinthorsdottir [a,b,*], P.E. Jardine [c], B.H. Lomax [d], T. Sallstedt [a]

[a] Department of Palaeobiology, Swedish Museum of Natural History, SE 104 05 Stockholm, Sweden
[b] Bolin Centre for Climate Research, Stockholm University, SE 109 61 Stockholm, Sweden
[c] Institute of Geology and Palaeontology, University of Münster, 48149 Münster, Germany
[d] School of Biosciences, University of Nottingham, Sutton Bonington, LE12 5RD Leicestershire, UK

ARTICLE INFO

Editor: Alan Haywood

*Keywords:*
Climate sensitivity
Paleo-$pCO_2$ reconstructions
Stomatal proxy
Climate change
ginkgo
Natural variability

ABSTRACT

The Ginkgoales, including the 'living fossil' *Ginkgo biloba*, are an important group for stomata-based palaeo-$pCO_2$ reconstructions, with long evolutionary lineages and an extensive, abundant fossil record. The stomatal proxy for palaeo-$pCO_2$ can improve our understanding of the exact relationship between $pCO_2$ and temperatures – Earth's climate sensitivity: a key measure of global warming by $pCO_2$. However, $pCO_2$ records from future climate analogues in the past, such as the mid-Miocene Climatic Optimum, seemingly underestimate $pCO_2$ – climate models cannot simulate the past temperatures with the only moderately elevated $pCO_2$ reconstructed by proxies. Either climate sensitivity must have been elevated, which has implications for future climate forecasts, or proxies underestimate $pCO_2$ due to additional environmental factors. Here we tested whether climate conditions impact stomatal parameters and thus $pCO_2$ reconstruction on a large global database of *G. biloba* leaves from all continents except Antarctica, spanning 12 climate zones. We reconstructed ambient $pCO_2$ using three stomatal proxy methods (stomatal ratio, transfer functions, Franks gas exchange model) and one stomata-independent isotope-based proxy for comparison ($C_3$ proxy). We found that the stomatal proxy methods reconstructed ambient $pCO_2$ reasonably well and uniformly, but that the $C_3$ proxy underestimated $pCO_2$. All the investigated stomatal parameters displayed an unexpectedly large variability, but no significant relationship with temperature, precipitation, or seasonality. Based on these results, the stomatal proxy is not influenced by climate and specifically does not systematically underestimate $pCO_2$ under high temperatures. Climate sensitivity was likely instead elevated during past global warming episodes, an urgent consideration in climate forecasts for our rapidly warming Earth.

## 1. Introduction

### 1.1. Looking at past climates to learn about the future

Atmospheric carbon dioxide concentration ($pCO_2$) has increased to 50% above pre-industrial levels (~280 ppm), with $pCO_2$ of 420 ppm measured at Mauna Loa for the first time in May 2021 (esrl.noaa.gov). Reducing uncertainties in future climate change forecasts is one of today's most important scientific challenges, but many significant problems are still unresolved. One of the most important is that the exact relationship between $pCO_2$ and temperature – climate sensitivity – remains poorly constrained (Huber et al., 2014; Hausfather, 2018; Farnsworth et al., 2019; Bloch-Johnson et al., 2021). The concept of climate sensitivity is defined in various ways, depending e.g. on the time scales involved. Equilibrium climate sensitivity (ECS) is defined as the long-term temperature increase caused by a doubling of $pCO_2$ after 'fast' feedbacks have fully set in, including changes in water vapour, cloud cover, snow and sea ice albedo, as well as perhaps smaller ice caps and glaciers (Hausfather, 2018). ECS is used for the ongoing Anthropogenic climate change, and evaluated at 3 °C as 'best estimate', with a 'very likely' range between 2 °C and 5 °C (IPCC, 2021), while some alternative climate sensitivity calibrations predict even larger increases in temperatures (Knutti et al., 2017). Earth system sensitivity (ESS) is the term for climate sensitivity on even longer timescales (palaeo-climate

* Corresponding author at: Department of Palaeobiology, Swedish Museum of Natural History, SE 104 05 Stockholm, Sweden.
*E-mail address:* margret.steinthorsdottir@nrm.se (M. Steinthorsdottir).

https://doi.org/10.1016/j.gloplacha.2022.103786
Received 27 October 2021; Received in revised form 4 March 2022; Accepted 11 March 2022
Available online 16 March 2022

sensitivity), and includes both 'fast' and 'slow' feedbacks, such as changes in continental ice sheets, ocean circulation and in Earth's surface properties through the re-distribution of vegetation cover (Royer et al., 2012; Knutti et al., 2017). ESS is generally considered to be elevated compared to ECS (Lunt et al., 2010; Royer et al., 2012; Hansen et al., 2013). While ESS is most often referred to when estimating paleo-climate change, ECS may also be appropriate to consider during transient, relatively short warming episodes in the past – hereafter, we use to the more general term of 'climate sensitivity'. It has been suggested that one of the reasons behind the difficulty in constraining climate sensitivity is that it may be state-dependent (Royer et al., 2007; Caballero and Huber, 2013): i.e. the warmer the background climate, the greater the temperature response for a given rise in $pCO_2$, in other words, the higher the climate sensitivity (Bloch-Johnson et al., 2021).

More accurate quantification of climate sensitivity against various boundary conditions is a crucial challenge in the effort towards better understanding the climate of our near future Earth. Since there is no precedence in instrumental records for the present and forecasted future climate, climate scientists must look back into the geological past to study various "future climate analogues" – periods of increasing $pCO_2$ and global warming, to study the relationship between $pCO_2$ and temperature, as well as feedbacks involved. The Cenozoic (~66–0 Ma) experienced several transient warm episodes with highly elevated temperatures and perturbations of the carbon cycle, superimposed on the dominant pattern of long-term cooling (Zachos et al., 2001; Cramwinckel et al., 2018; Westerhold et al., 2020). Three Cenozoic warm episodes are particularly important to study according to the IPCC. These are referred to as 'Paleoclimate Reference Periods' and include the early Eocene Climatic Optimum (EECO, ~50 Ma), when $pCO_2$ was >1000 ppm and global mean temperatures were ~ 13 °C warmer than today (Caballero and Huber, 2013; Burke et al., 2018; Inglis et al., 2020); the mid-Pliocene Warm Period (PWP, 3.3–3.0 Ma), which experienced what is lower than present day $pCO_2$ (~400 ppm), and global warming of 2–3 °C (Lunt et al., 2010; Pagani et al., 2010; Haywood et al., 2016; Burke et al., 2018), and the mid-Miocene Climatic Optimum (MCO, ~16.9–14.7 Ma) – included for the first time in the 6th Assessment Report. Significant differences in geography, flora and fauna relative to the modern day make the EECO an inappropriate future analogue. The PWP is much younger and more similar to modern Earth in myriad ways, yet the fact that PWP $pCO_2$ has already been surpassed also renders it somewhat imperfect. PWP-like climate is predicted as early as 2030 (Burke et al., 2018) and may in fact be a near-future 'best-case scenario', prevailing only if emissions are drastically reduced immediately. This is possible only if societies meet the targets of the Paris Agreement to limit global warming to below 2 °C, which at present seems unlikely to succeed (Hausfather, 2018). Unmitigated greenhouse gas emissions move us quickly beyond the PWP state and pushes the Earth into a potentially vulnerable position where many tipping points of subsystems may be triggered, such as e.g. those of glaciers, sea ice, coral reefs, deserts, and forest biomes, which may disappear or become permanently destabilized (Schellnhuber et al., 2016).

The Miocene (~23–5 Ma), and in particular the MCO, has recently been suggested as an appropriate 'intermediate' deep-time climate analogue (see Steinthorsdottir et al., 2021a for review). During the MCO, paleogeography and biota were reasonably similar-to-modern, but temperatures were in the upper range of predictions for 2100 using the IPCC's 'Representative Carbon Pathways' (RCP) at up to ~7–8 °C warmer than modern in mid-latitude regions. The MCO climate is thus an important case study for assessing and improving the predictive accuracy of numerical climate models – the same models that are used to simulate future climates.

### 1.2. Proxies vs current understanding of climate sensitivity

The marine and terrestrial palaeo-temperature records are considered highly reliable (see e.g. Zachos et al., 2001; Cramwinckel et al., 2018; Westerhold et al., 2020). However, a key research problem remains unresolved in relation to Cenozoic warm periods such as the Paleocene-Eocene Thermal Maximum (PETM), the EECO and the MCO, namely that proxies seemingly underestimate $pCO_2$ relative to climate models. The moderate $pCO_2$ recorded by proxies during these warm intervals cannot be reproduced with climate models. For example, most existing MCO $pCO_2$ reconstructions record <450 ppm (i.e. similar to moderately higher $pCO_2$ than modern) and at most ~550 ppm, even for the peak warmth of the MCO (e.g. Royer, 2003; Royer et al., 2001; Kürschner et al., 2008; Grein et al., 2013; Zhang et al., 2013; Greenop et al., 2014; Foster et al., 2017; Steinthorsdottir et al., 2021a, Steinthorsdottir et al., 2021b). This has proved difficult to reconcile with models, as climate model simulation can only reproduce MCO temperatures at ~800 ppm (Goldner et al., 2014), considerably higher than reconstructed $pCO_2$. These observations lead to several alternative hypotheses, the two most prominent being that either the climate system is more sensitive than we currently believe and relatively minor $pCO_2$ changes can drastically reshape Earth's climate, or proxies underestimate $pCO_2$ and it was in reality higher during the MCO (or possibly some combination of both). A third possibility is that proxies are accurately reconstructing $pCO_2$, but the climate models currently in use are not adequately simulating $pCO_2$-independent positive forcings, such as those caused by changes in ocean circulation, terrestrial albedo, as well as in cloud cover and aerosol load (Huber, 2013). Faced with the prospect that perhaps our future Earth may become much warmer than presently predicted, it is important to try to resolve this enigma.

Modelling studies have repeatedly suggested that equilibrium climate sensitivity was elevated relative to modern during Cenozoic warm episodes such as the PETM (Shaffer et al., 2016; Inglis et al., 2020) and the EECO (Anagnostou et al., 2016; Cramwinckel et al., 2018; Inglis et al., 2020), but depressed during colder past periods, such as the Last Glacial Maximum (Inglis et al., 2020). The MCO is understudied in this respect, but displays similar temperature-$pCO_2$ discrepancy as the other Cenozoic warm periods. On the other hand, recent re-evaluations of the marine boron (Sosdian et al., 2018) and alkenone (Stoll et al., 2019) $pCO_2$ proxies reconstructed MCO $pCO_2$ of ~800 ppm, bringing $pCO_2$ in line with concentrations needed by climate models to reconstruct MCO temperatures; however, both proxy recalibrations need further testing (Steinthorsdottir et al., 2021a). Here we test another important paleo-$pCO_2$ proxy, the stomatal proxy, to investigate whether it underestimates $pCO_2$ under certain conditions, such as under higher temperatures.

### 1.3. Reconstructing palaeo-$pCO_2$ with plants

Land plants grow in direct contact with ambient atmospheric $pCO_2$ and are constantly involved in gas exchange with the atmosphere via their leaf stomata. This is in contrast to marine organisms, where the recording of any $pCO_2$ signal must be filtered through multiple complex environmental parameters, such as the surrounding water's temperature, pH value and level of salinity, as well as the organisms' growth rate and chemical composition (Foster et al., 2012; Anagnostou et al., 2016; Greenop et al., 2014; Sosdian et al., 2018; Stoll et al., 2019). One of the most widely used proxies for reconstructing $pCO_2$ in the past is the stomatal proxy (Beerling and Royer, 2011; IPCC, 2021), which is principally rooted in the inverse relationship that exists between the density of stomata and $pCO_2$ (Woodward, 1987; see Section 1.5 below for detail). Similarly to other proxies, the stomatal proxy as currently calibrated often seemingly underestimates $pCO_2$ in the Cenozoic (Beerling and Royer, 2002; Wang et al., 2015; Steinthorsdottir et al., 2016a, 2016b; Steinthorsdottir et al., 2019a; Steinthorsdottir et al., 2021b). Plants in the orders Ginkgoales and Coniferales (ginkgos and conifers hereafter) radiated in the Mesozoic (252–66 Ma), when $pCO_2$ was mostly ~500–1000 ppm, with transient excursions >1500 ppm (Beerling and Royer, 2011; Steinthorsdottir et al., 2011; Franks et al., 2014; McElwain et al., 2016). As $pCO_2$ decreased during the late Cretaceous and

Cenozoic, angiosperms (flowering plants) rapidly diversified to become the dominant land plants (Friis et al., 2011). Angiosperm fossil leaves are more common than ginkgo and conifer leaves in most Cenozoic – including Miocene – deposits, and have thus been used for the bulk of stomatal proxy $pCO_2$ reconstructions. However, angiosperms consistently underestimate Cenozoic $pCO_2$ (e.g. Kürschner et al., 2008; Haworth et al., 2010; Steinthorsdottir et al., 2016a; Steinthorsdottir et al., 2019b; Steinthorsdottir et al., 2021a), to the extent that a correction factor of 150–200 ppm has been suggested for the common Cenozoic fossil plant taxon Lauraceae at above ambient $pCO_2$ based on inference models applied to herbarium and experimental datasets (Kürschner et al., 2008). In addition, it has repeatedly been shown that many living angiosperms have a ceiling of response (i.e., they no longer reduce their stomatal densities) to $pCO_2$, which is sometimes as low as ~350 ppm (Woodward, 1987; Beerling and Chaloner, 1993; Kürschner et al., 1996; Wagner et al., 1996). Because the stomatal proxy relies on the comparison between modern and fossil plant relatives, this response ceiling may limit the angiosperms' potential to accurately reconstruct elevated palaeo-$pCO_2$. The mechanisms behind this are not well understood, but recently differences in physiological traits, leaf conductance and photorespiration between angiosperms and gymnosperms have been suggested (Yoitis and McElwain, 2019; Hare and Lavergne, 2021). Ginkgos and conifers, on the other hand, originated and evolved under hothouse, high-$pCO_2$ conditions and many of their modern relatives seem to uphold the affinity for high $pCO_2$. For example, rather than having a relatively low ceiling of response, some conifers respond to much higher $pCO_2$ and some only begin reducing their stomatal densities in response to $pCO_2$ at >400 ppm (Kouwenberg et al., 2003; Haworth et al., 2010), and *G. biloba* continues responding at >500 ppm (Beerling et al., 1998; Barclay and Wing, 2016; Yoitis and McElwain, 2019). Ginkgo and conifer stomatal proxy $pCO_2$ reconstructions from the Mesozoic are furthermore usually fully in line with coeval temperature reconstructions, chemical proxies, isotope records and geochemical modelling (e.g. McElwain et al., 1999; Haworth et al., 2005; Steinthorsdottir et al., 2011, 2016b; Steinthorsdottir and Vajda, 2015; Wu et al., 2016; Mays et al., 2015; Slodownik et al., 2021).

### 1.4. *Ginkgo biloba: The "living fossil"*

Ginkgoales remain the most important group for stomata-based reconstructions of palaeo-$pCO_2$, due to its long lineages and the extensively demonstrated stomatal response of *G. biloba* – the sole living representative of the previously much more diverse taxon (Fig. 1). As a group, Ginkgoales has shown a remarkable evolutionary and ecological stability, with close ginkgo relatives found abundantly in the fossil record as far back as the Permian (~270 million years ago) (Royer et al., 2003; Crane, 2013; Guan et al., 2016). Today *G. biloba* is dispersed globally, growing on all continents except for Antarctica, and has been used most often of any species as a nearest living equivalent for palaeo-$pCO_2$ reconstruction using fossil ginkgos. However, in most previously published studies using *G. biloba* for this purpose, the number of specimens (leaves, trees) and geographical collection sites have been limited, most often to several leaves from fewer than ten trees at one or two sampling sites, or a small number of trees growing for short time spans in experimental chambers (Beerling et al., 1998; Chen et al., 2001; Retallack, 2001; Royer et al., 2001; Royer, 2003; Beerling et al., 2009; Barclay and Wing, 2016; Retallack and Conde, 2020). In order to refine the ginkgo stomatal proxy, it needs to be better understood whether additional environmental factors, apart from $pCO_2$, significantly affect stomatal parameters of living – and therefore presumably the macro- and micro-morphologically near-identical fossil – ginkgos. Due to the hypothesis of heightened climate sensitivity and ecosystem responses under warmer conditions, we considered the effect of elevated temperature particularly pertinent to test.

### 1.5. *The stomatal proxy for palaeo-$pCO_2$ reconstruction*

Stomata are small pores on leaf surfaces (Fig. 1), which are used for gas-exchange: $CO_2$ is acquired for photosynthesis, and at the same time water vapour and oxygen are lost by diffusion. When a lot of $CO_2$ is available in the atmosphere ($pCO_2$ is high), most woody plants react by reducing the density of stomata on their leaves, to preserve water. This inverse relationship between $pCO_2$ and stomatal density ($SD = N_{stomata}/mm^2$), or the now more commonly used stomatal index ($SI\ (\%) = N_{stomata}/(N_{stomata} + N_{epidermal\ cells})$), can consequently be used to reconstruct $pCO_2$ in the past. The stomatal proxy was originally established based on empirical studies of herbarium leaves, showing that modern tree species have responded to the anthropogenic rise in $pCO_2$ by reducing stomatal densities (Woodward, 1987). Since then, the inverse relationship has been confirmed in numerous experimental studies (e.g. Beerling et al., 1998; Kürschner et al., 2008; Barclay and Wing, 2016; Hincke et al., 2016) and the physiological mechanisms as well as signalling and genetic pathways involved have been identified (Gray et al., 2000; Lake et al., 2001; Frommer, 2010). The stomatal proxy has been successfully applied to a wide variety of plant taxa from disparate geological and ecological settings from the Palaeozoic (from ~350 million years ago) until today (see Foster et al., 2017 and McElwain and Steinthorsdottir, 2017 for review).

Three main methods are currently in use. Firstly, the simple empirical stomatal ratio method utilizes the ratios between stomatal densities of fossil leaves and their nearest living relatives or equivalents grown under known $pCO_2$ to semi-quantitatively reconstruct palaeo-$pCO_2$ (McElwain, 1998). Secondly, the likewise empirical transfer function method (now sometimes referred to as the stomatal index method) uses herbarium and/or experimental datasets of responses to variations in $pCO_2$ to construct regression curves on which fossil stomatal densities from nearest living relatives (ideally con-specific) can be plotted to infer palaeo-$pCO_2$ (e.g. Kürschner et al., 2008; Barclay and Wing, 2016). Finally, the more recently developed mechanistic gas-exchange models are conceived to be more taxon-independent, but are still based on morphological and plant physiological measurements from closely related plants, as well as input of additional parameters, such as leaf $\delta^{13}C$ (Franks et al., 2014; Royer et al., 2019; Konrad et al., 2017, 2020). All three methods thus rely on comparisons between fossil plants and their living relatives and, importantly, the records produced using these different methods largely agree with each other (see Franks et al., 2014; McElwain et al., 2016; Montañez et al., 2016; McElwain and Steinthorsdottir, 2017; Steinthorsdottir et al., 2019a; Zhou et al., 2020; Steinthorsdottir et al., 2021b). Here we tested all three proxy methods – the stomatal ratio method, transfer functions and the Franks gas-exchange model, and additionally applied a stomata-independent method – the $C_3$ proxy, which utilizes fossil plants' stable carbon isotope discrimination ($\Delta^{13}C$) to reconstruct palaeo-$pCO_2$ (Schubert and Jahren, 2012, 2015). This comparison is made to highlight the different approaches used to calculate palaeo $pCO_2$ from terrestrial settings but we note that previously published studies have suggested only a very weak predictive relationship between $pCO_2$ and $\Delta^{13}C$ (Diefendorf et al., 2015; Lomax et al., 2019; Stein et al., 2019; Schlanser et al., 2020; Stein et al., 2021). The $C_3$ proxy has recently been updated to use $\delta^{13}C_{plant}$ rather than $\Delta^{13}C$ as the main predictor variable (Cui et al., 2020), but the underlying equations still rely on the modelled relationship between $\Delta^{13}C$ and $pCO_2$, and result in broadly similar $pCO_2$ estimates (Cui et al., 2020; Jardine and Lomax, 2021).

### 1.6. *Global vs local $pCO_2$*

Almost all of the ginkgo trees studied here grow in urban or suburban settings around the world. We focused on obtaining leaves from trees growing in city parks or in suburban recreational areas, mostly avoiding street trees near city centres – however, the local $pCO_2$ conditions need to be considered. Although $pCO_2$ is usually indicated as a single value for

each year (in this case ~405–407 ppm for 2017–2018), based on the average measured in the pristine remote settings at Mauna Loa, there is considerable seasonal variation in $pCO_2$. This variation is mostly linked to the role plants and other photosynthesizers play in the short-term carbon cycle, as well as a diurnal fluctuation, with highest $pCO_2$ during the night and lowest during the day. In the Northern Hemisphere, where most carbon cycle activity takes place, monthly averaged $pCO_2$ peaks around May–June, falls ~6–7 ppm during the Northern Hemisphere growing season to minimum values around September–October, before rising again ~8–9 ppm during the winter season to the next spring maximum (see www.noaa.gov). The Southern Hemisphere $pCO_2$ cycle is less pronounced, and $pCO_2$ is slightly lower than in the Northern Hemisphere, although only by a few ppm (Keeling et al., 2010; Tomizuka, 2013).

Satellite $pCO_2$ measurements frequently show highly elevated $pCO_2$ over densely populated areas in the Northern Hemisphere, but we cannot be confident that this satellite data reflects conditions on the ground due to difficulty of estimating the vertical profile of greenhouse gases from space and overall challenges with accuracy of satellite-based measurements (e.g. Yue et al., 2016). A more complicated picture emerges when considering $pCO_2$ in the geographically patchy human-dominated urban and suburban environments. It has been shown that, in addition to the well-known urban heat island effect (first reported by Manley, 1958), cities are associated with $pCO_2$ domes, with the highest $pCO_2$ above the busiest part of the city centres (Idso et al., 1998, 2001). Urban $pCO_2$ can temporarily be >100 ppm higher than the global average, although it is usually less elevated (Idso et al., 2002; George et al., 2007; Imasu and Tanabe, 2018; Xueref-Remy et al., 2018), and highly elevated $pCO_2$ is often extremely localized (Soegaard and Møller-Jensen, 2003; Pigliautile et al., 2020). It has been shown that the urban domes' primary source of $CO_2$ is anthropogenic emissions, often with traffic as the largest single source, and that the dome is strongest on weekdays, on winter nights with little or no wind, in the presence of strong temperature inversions (see e.g. Haiduc and Beldean-Galea, 2011 for review). $CO_2$ fluxes are dependent on the cities' density and structure, as well as the continental topography with the associated meteorological features, such as wind direction and speed, atmospheric humidity, turbulence and thermal inversions (Turnbull et al., 2015; Xueref-Remy et al., 2018). Studies that recorded the average heightened urban $pCO_2$ compared to rural or global background values over some months or years mostly reported average $pCO_2$ of ~20–60 ppm higher at the urban sites, with shorter-term spikes in $pCO_2$ and large variations (Gratani and Varone, 2005; Moriwaki et al., 2006; George et al., 2007; Imasu and Tanabe, 2018).

The exploration of how climate influences both stomatal features and carbon isotope discrimination has been the subject of previous studies. For example, Sun et al. (2003) examined how climate effected stomatal characteristics (SD and SI) in *G. biloba* from three sites in China (Lanzhou, Beijing, and Nanjing) and compared $\Delta^{13}C$ values from these Chinese locations to data from London, UK. Whilst the authors showed minimal variation is SD and SI across the climate gradient, these differences were not tested for and how these factors influenced $pCO_2$ prediction was not considered. More recently Yan et al. (2017) sought to explore the relationship between stomatal parameters and climate through meta-analysis. Their data analysis suggested a complicated relationship between stomatal characteristics and climate. For example, they noted that elevated temperature increased abaxial SD and SI but did not influence adaxial SD or SI, which they reported as being at odds with some existing studies, e.g. Loveys et al. (2002), while consistent with others (Reddy et al., 1998; Luomala et al., 2005. The meta-analysis (Yan et al., 2017) combined both field and experimental data, and again did not consider how variation in stomatal parameters driven by climate may feed through to influence the accuracy and precision of stomatal based $pCO_2$ proxies.

Here, we use the Earth as a form of an experimental growth chamber to test the effects of environmental factors other than $pCO_2$ on the stomatal parameters and other key traits of *G. biloba* grown in natural conditions (i.e. not in growth chambers) at approximately equal $pCO_2$, but in a wide variety of climate regimes. These data are then used to assess how climate variables feed through to impinge on the utility of various methods to predict $pCO_2$. When making $pCO_2$ predictions from our global ginkgo database, we highlight that due to the complexity of determining local $pCO_2$ as described above, we use the global average $pCO_2$ for 2017 of 405 ppm as the minimum value. We note, however, that many of the trees growing in urban environments most likely experienced higher $pCO_2$ conditions, and set the maximum average $pCO_2$ to 450 ppm.

## 2. Material and methods

### 2.1. Leaf database and laboratory methods

The full dataset comprises 667 *G. biloba* leaves derived from 141 trees growing in 18 countries, on all continents except Antarctica, and across 12 climate zones using the Köppen climate classification scheme (Fig. 2, Tables S1 and S2). As far as we are aware, no *G. biloba* grow in group A: Tropical/megathermal climates, nor E: Polar climates, but the trees studied here represent group B: Dry climates (including Bwk: cold desert; BWh: hot desert; Bsh: hot semiarid; Bsk: continental semiarid/steppe;), group C: Temperate/mesothermal climates (including Csa: Mediterranean, mild/hot summer; Cfa: warm temperate rainy or humid subtropical; Cfb: warm temperate, oceanic; Cwa: humid subtropical, monsoon; Cwb: temperate, monsoon) and group D: Continental/microthermal climates (including Dwa: continental mild/hot summer/monsoon; Dfa: humid continental, hot summer; Dfb: humid continental, mild summer). Altitude ranges from 3 to 2470 m.a.s.l. (meters above sea level), the mean annual temperature of the sampling localities from 7.2 to 25.5 °C, with maximum summer temperatures ranging 19.0 to 40.5 °C and minimum winter temperatures −19.3 to 10.3 °C, while the total annual precipitation ranges from 119 to 2573 mm/year – classified as evenly distributed, summer wet, winter wet, or arid (Fig. S1 and Table S2). (See Fig. 2.)

The leaves studied here all derive from trees that have been propagated and planted by humans, i.e. the trees may in many cases be growing outside their natural range. *Ginkgo biloba* is endemic to China, but only grows in the wild in fragmented populations in former glacial refugia in the Dalou Mountains, SW China (Tang et al., 2012). The largest subsets within the dataset come from China (75 trees) and Europe (37 trees). One tree, 'Goethe's ginkgo' from Jena, Germany (JenT1), counts as two specimens, with five leaves from the male main tree (JenT1a), and five leaves from a female branch (JenT1b), that had been grafted onto the main tree. Leaf collection took place in 2017 and 2018 and was "citizen scientist" assisted, with most leaves sent by mail to the Swedish Museum of natural History. The aim was retrieving five leaves from each tree, which was achieved for 113 trees (80% of the database, with five leaves each for specimens JenT1a and JenT1b). Four leaves were collected from each of 11 trees, three leaves from 13 trees and two leaves from four trees. To test for the impact of generating data from fewer than five leaves per tree, as well as the presence of four street or garden trees (as opposed to those growing in parks and recreation areas) in the dataset, we compared the distributions of the main measured parameters with and without these trees included. Since the overall distributions were highly similar, and Kolmogorov-Smirnov tests of equality of distributions indicated no significant differences (see Fig. S2 for plots of the distributions and Kolmogorov-Smirnov test results, all of which are not statistically significant), we have included all sampled trees in the analysis. To test variability within and between localities, as well as intra and inter tree variability, we included leaves from more than one tree per locality when possible, resulting in 11 localities represented by two trees, 10 by three trees, five by four trees, five by five trees, and one locality each represented by six and seven trees (see Table S2).

**Fig. 1.** Extant and fossil ginkgo leaves. To the left, living *Ginkgo biloba* growing outside the Swedish Museum of Natural History and fossil *Ginkgo cordilobata* leaves from the Lower Jurassic (ca. 200 million year ago) of Afghanistan (photo and collage: Sara Schesny). To the right, cuticle morphology of *G. biloba*, showing stomata and epidermal cells. Scalebar = 100 μm. (photo: Margret Steinthorsdottir).

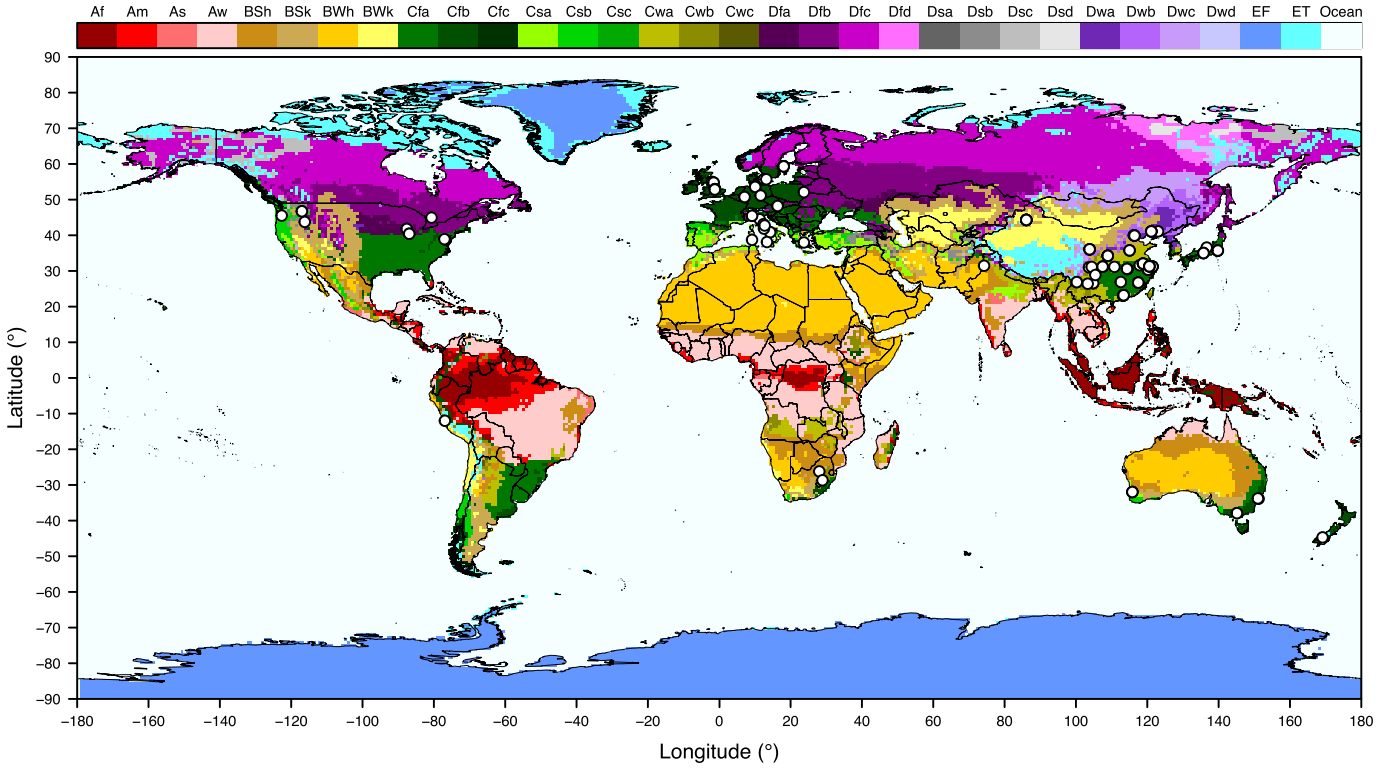


**Fig. 2.** A world map showing the distribution of Köppen vegetation-based climate zones and the ginkgo collection localities (white circles). Map produced using code and data downloaded from http://koeppen-geiger.vu-wien.ac.at/present.htm (Kottek et al., 2006; Rubel et al., 2017). (For interpretation of the references to colour in this figure legend, the reader is referred to the web version of this article.)

All leaves were individually tagged with tree ID and leaf number, and sampled for carbon isotope analysis. The first subset of leaves (111) were photographed and weighed, in order to record leaf mass per area (LMA), as well as perimeter to determine shape factor and compactness, as previous studies have recorded changes to LMA and leaf shape relative to global climate and during past episodes of climate warming (Peppe et al., 2011; Bacon et al., 2013; Soh et al., 2017). However, an initial analysis yielded no discernible trends for these factors, and was not pursued further, but the data are provided in supplements for completeness (Tables S1 and S3). A rectangle of ~1 × 1 $cm^2$ was cut out of the mid-lateral part of each leaf, using scissors, and these were then macerated in a 50/50 solution of glacial acetic acid ($CH_3COOH$) and hydrogen peroxide ($H_2O_2$) in test tubes for several days on a hot plate at approximately 75 °C inside a fume hood. When all mesophyll was dissolved, the upper and lower cuticles were separated in a petri dish containing distilled water using small brushes and dissection needles under a stereo microscope. The lower (abaxial – stomata bearing) cuticle samples were stained with a staining agent (Sudan IV) and mounted on permanent slides using Kaiser's gel (glycerine gelatine). For one leaf per tree, the upper (adaxial – astomatous) cuticle was also stained and mounted following the procedure above. The leaf cuticle abaxial surface were photographed at 200× magnification using a Leica microscope with a mounted Leica camera (DF310 FX) and associated software (LAS v3.8) and all subsequent analyses were performed on the image database, using the public domain Java image processing program ImageJ (www.imagej.nih.gov). Five abaxial and one adaxial images per leaf were recorded, resulting in 3335 abaxial and 142 adaxial images. The images were annotated with grids, delimiting areas of 300 × 300 μm, and stomata as well as epidermal cells within each of on average five grids per leaf were counted. Pore length and guard cell width were measured on ten stomata per leaf.

### 2.2. Data analysis

#### 2.2.1. Analytical tools and climate input data

Data analysis was carried out using R *v*. 4.1.1. (R Core Team, 2021) with the packages mgcv *v*. 1.8–36 (Wood, 2017), ppcor *v*. 1.1 (Kim, 2015), raster *v*. 3.4–13 (Hijmans, 2021), rasterVis *v*. 0.51.0 (Lamigueiro and Hijmans, 2021), rworldxtra *v*. 1.01 (South, 2012) and rgdal *v*. 1.5–23 (Bivand et al., 2021). We used climate estimates from the CRU TS (Climatic Research Unit gridded Time Series) dataset v. 4.05 (Harris et al., 2020; available from the CEDA Archive https://archive.ceda.ac.uk, or https://crudata.uea.ac.uk/cru/data/hrg/cru_ts_4.05/), which provides monthly climate data for the years 1901 to 2020 on 0.5 × 0.5° grids. From the CRU dataset we generated estimates for mean, minimum and maximum annual temperature, total annual precipitation (TAP), and mean annual vapour pressure deficit (VPD), for each sampled location and year. We calculated VPD using Eqs. 1, 6, 7, and 8 in Yuan et al. (2019), using the vapour pressure estimates in the CRU dataset along with the mean annual temperature (MAT) and elevation data for each locality. We estimated seasonal variability in the climate parameters via temperature annual range (maximum minus minimum annual temperature), temperature seasonality (standard deviation of monthly mean temperature) and precipitation seasonality (coefficient of variation of monthly precipitation), which correspond with the WorldClim bioclimatic variables seasonality parameters (https://www.worldclim.org/data/bioclim.html). Mean, minimum, and maximum annual temperature are all positively correlated in our dataset (Fig. S1), and so we limited our analyses to MAT. Similarly, temperature annual range and seasonality are strongly positively correlated, and so we focused on temperature annual range as an indicator of seasonal variability.

Due to the lack of reliable and accessible data on local $pCO_2$ at the *G. biloba* collection sites (see Section 1.5), we catalogued the sites' degree of urbanization according to population size, as a rough measurement of likely elevated $pCO_2$ at the more urban sites. We compiled population size and density data for our sampled localities from internet resources (Table S2). Different countries use significantly different population categories; here we followed the basic definitions of towns and cities used by the World Bank, as well as the most commonly used regional definitions for the remaining categories. In addition to analysing population size as a continuous variable, we binned the localities into the following classes: rural (no or very few inhabitants), village ($< 5$ thousand inhabitants), town ($\geq 5$ thousand and $< 50$ thousand inhabitants), small city ($\geq 50$ thousand and $< 2$ million inhabitants), large city ($\geq 2$ million and $< 10$ million inhabitants), megacity ($\geq 10$ million inhabitants) (Table S2).

#### 2.2.2. Stomata- and leaf-based $pCO_2$ reconstructions

We use several sets of previously published *G. biloba* stomatal index-$pCO_2$ pairs to reconstruct modern $pCO_2$ in the stomatal ratio method, including those of Beerling et al. (1998), McElwain et al. (1999), and Royer (2003). We note that it has been recommended that early stomatal index results be viewed with caution, because that subsequent progress in data collection, including sampling design, imaging and counting methods may render them unreliable (Barclay and Wing, 2016). Two more recent studies which may be considered more reliable record stomatal index of 10–12% at 375 ppm (Xie et al., 2009) and 11.3% at 390 ppm (Steinthorsdottir et al., 2011). The former study is based on >25 leaves from five localities in China, whereas the latter is based on 100 leaves from one tree in Ireland.

Considerable effort has been made over the last two decades to produce a reliable, universally applicable transfer function for *G. biloba*, using herbarium and/or experimental datasets. We tested all previously published transfer functions using our global ginkgo dataset (Beerling et al., 2002; Retallack, 2002; Royer, 2003; Wynn, 2003; Retallack, 2009; Barclay and Wing, 2016). We note again that Barclay and Wing (2016) recommended excluding older transfer functions due to progress in the field making them redundant, but since no transfer function so far has been able to reproduce highly elevated $pCO_2$ convincingly, we consider that this is an ongoing effort.

To estimate $pCO_2$ using the Franks model, we used the Franks model v.2 R code provided in the supplementary material to Kowalczyk et al. (2018). We primarily focused on using the input parameters provided by Franks et al. (2014) for ginkgo, using $\delta^{13}C_{air} = -8.5$, $pCO_2\_0 = 400$, A0 = 5.9, CiCa0 = 0.57, gb = 2, s1 = 1, s2 = 1, s3 = 0.6, s4 = 0.2, s5 = 0.013, and fixed_A = "yes" because the A0 value given in Franks et al. (2014) was based on direct measurements from ginkgo trees. However, to provide a comparison and test the sensitivity of variations in the input parameters, we used alternative values for ginkgo provided by Kowalczyk et al. (2018), which differ in the present-day photosynthetic rate (parameter A0) and $C_i/C_a$ value (parameter CiCa0), with A0 = 8.09 and CiCa0 = 0.53.

For the $C_3$ model, we generated $pCO_2$ estimates using both the original $\Delta^{13}C$-based version (Schubert and Jahren, 2012, 2015; Cui et al., 2020) and the updated $\delta^{13}C$ version (Cui et al., 2020). In both cases we used the model parameters A = 28.26, B = 0.22 and C = 23.9, and used the Holocene baseline values of $\delta^{13}C_{org} = -25.0‰$, $\delta^{13}C_{air} = -6.4‰$ and $pCO_2 = 270$ ppm given in Cui et al. (2020) to reconstruct current ambient $pCO_2$.

For both the Franks model and the $C_3$ model, 68% and 95% confidence intervals were generated by Monte Carlo resampling of the input parameters and their associated errors. In each case the confidence intervals were based on 10,000 resamples, with estimates under 0 ppm and above $10^6$ ppm removed before the 2.5th, 16th, 84th and 97.5th percentiles of the distribution were calculated, along with the median (the 50th percentile) which provides the $pCO_2$ estimate (Table S4).

To compare the measured leaf parameters and $pCO_2$ estimates against climate variables we used a combination of pairs plots, correlation tests, and additive model smoothers to assess linear or non-linear relationships between variables (Zuur et al., 2009). The additive models were estimated using restricted maximum likelihood (REML); because these were primarily used for data exploration formal model validation and selection was not carried out.

## 3. Results

### 3.1. Key parameters

Across the dataset, the within-tree mean values for stomatal density (SD) ranges from 92.50 to 286.84 stomata/mm$^2$ (mean 189.02, standard deviation 37.57, $n = 142$), while stomatal index (SI) within-tree means range from 6.56 to 12.86% (mean 9.27, standard deviation 1.41, $n = 142$). Within-tree mean stomatal guard cell width (GCW) ranges from 4.33 to 7.79 μm (mean 5.92, standard deviation 0.65, $n = 142$), and the stomatal pore length (PL) within-tree means range from 8.16 to 13.37 μm (mean 10.20, standard deviation 0.86, $n = 142$). $\delta^{13}C$ ranges from −31.25 to −25.82‰ (mean − 28.47, standard deviation 1.25, $n = 142$). SD and SI are highly positively correlated ($r = 0.70$, $p < 2.2 \times 10^{-16}$) with one another, and stomatal density shows a weak negative correlation with GCW ($r = -0.20$, $p = 0.02$) and pore length ($r = -0.25$, $p = 0.003$) (Fig. S3). None of the stomatal variables are obviously correlated with $\delta^{13}C$ (Fig. S3).

### 3.2. Testing variability in key parameters

For the four stomatal parameters the among-tree standard deviation is typically higher than the within-tree standard deviation (i.e. there is more variability among trees than among leaves of the same tree) although for all parameters some trees in the dataset exceed the among-tree standard deviation (Fig. S4). The within-tree standard deviations of SD and SI are positively correlated but otherwise there are no obvious relationships among these variables (Fig. S5). For the seven localities with five or more sampled trees, the within-locality, among-tree standard deviation varies from 34 to 138% of the dataset-wide among-tree

standard deviation for $\delta^{13}C$, 45 to 95% of the among-tree standard deviation for SD, 27 to 89% of the among-tree standard deviation for the SI, 9 to 73% of the among-tree standard deviation for GCW and 29 to 115% of the among-tree standard deviation for PL (Fig. 3). Neither the Europe nor China geographic subsets show any systematic differences from the whole dataset parameter distributions (Fig. S6). Pairwise two-sample Kolmogorov-Smirnov tests only indicate one significant difference between distributions at a Bonferroni-corrected α value of 0.05/3 = 0.017, which is for GCW between the China and Europe subsets, and is probably linked to the bimodal distribution of GCW measurements in the European data (see Fig. S6 for statistical test results).

### 3.3. Testing the influence of climate on stomatal parameters

There is limited evidence for a climatic effect on the stomatal parameters, with only weak positive or negative correlations between MAT or TAP and the tree means or standard deviations (Fig. 4, S3 and S5). $\delta^{13}C$ correlates negatively with TAP (Spearman's $rho = -0.55$, $p = 8.2 \times 10^{-13}$) and MAT (Spearman's $rho = -0.35$, $p = 1.9 \times 10^{-5}$), however, resulting in lower $\delta^{13}C$ values in Köppen zone C relative to zones B and D (Fig. 4 and S7). The relationship between $\delta^{13}C$ and TAP is consistent with that recorded in previous analyses (e.g. Kohn, 2010), and the weaker relationship between $\delta^{13}C$ and MAT may just be a reflection of the positive correlation between TAP and MAT in this dataset. Consistent with this interpretation, a partial correlation test of MAT and $\delta^{13}C$ while accounting for TAP does not support an independent correlation between these variables (Spearman's $rho = -0.10$, $p = 0.24$). There are no obvious relationships between the measured parameters and temperature or precipitation seasonal variation, or VPD (Figs. S3 and S5). Similarly, there are no clear relationships between the measured parameters and population size, apart from trees from the two largest cities (Tokyo and Shanghai) being limited to more negative $\delta^{13}C$ values (Fig. S8), which may be due to anthropogenic enrichment of the $CO_2$ isotopic signature (Graven et al., 2020).

Limiting the analysis to either the Europe (Fig. S9) or China (Fig. S10) geographic subsets produces similar results to the full dataset, although there are differences related to the climate space occupied for these samples and the impact this has on the measured parameters (particularly $\delta^{13}C$). The European data covers a narrower range of MAT (7.16 to 18.38 °C) and TAP (333.3 to 1128.2 mm/year) with a limited correlation between them (Fig. S9), while the China data extends over a broader climatic range (MAT 8.3 to 23.1 °C, TAP 160.2 to 1833.5 mm/year) covering a gradient from cold, dry climates to warm, humid ones (Fig. S10). In both cases there is limited evidence for a relationship between stomatal parameters and climate, but in the China data there is a stronger, more linear relationship between $\delta^{13}C$, TAP and MAT relative to the full dataset (Figs. S10 and S11).

### 3.4. Impact of leaf parameter variability on proxy-calibrated $pCO_2$

We have applied the four different proxy methods to our global ginkgo database to generate estimates of $pCO_2$ (Table S4). This framework allows us to compare proxy predicted $pCO_2$ to globally averaged $pCO_2$ with a range in measured $pCO_2$ to reflect issues linked to urbanization. Overall, we found that the different stomatal ratio calibrations produce a wide range of $pCO_2$ estimates when applied to the ginkgo dataset, with each calibration generating values ranging over 250–350 ppm and with median values that over- or underestimate ambient $pCO_2$ by up to 100 ppm (Fig. 5). The Royer (2003) ratio produces the value most reflective of modern $pCO_2$ at ~400 ppm. Results using the ratios in Xie et al. (2009) and Steinthorsdottir et al. (2011) show elevated $pCO_2$ of ~490–500 ppm, which is outside of the range considered ambient here. Calculating the overall median of the stomatal ratio $pCO_2$ estimates gives a value of 428 ppm, which is in good agreement with current ambient $pCO_2$. We note that here we are testing our global dataset's *Ginkgo biloba* SI against previously published SI also deriving from modern ginkgos, not evaluating how well the stomatal ratio method reconstructs palaeo-$pCO_2$ using fossil ginkgos.

The median estimates produced by the transfer functions almost uniformly underestimate ambient $pCO_2$ by ~50–100 ppm, in particular when noting the prevailing higher urban $pCO_2$ of up to ~450 ppm (Fig. 6). The range of $pCO_2$ estimates produced by each transfer function covers ~400 to >1000 ppm. Again, we are testing transfer functions based on modern ginkgo SI dataset against each other and not commenting on their usefulness in reconstructing palaeo-$pCO_2$ with fossil ginkgos, although we note with interest that the large majority of the transfer functions underestimate modern $pCO_2$.

The Franks model using the input parameters from Franks et al. (2014) converges quite well on ambient $pCO_2$ in terms of the median estimated value and the interquartile interval (lower quartile 365 ppm, median 402 ppm, upper quartile 456 ppm), but nevertheless produces a tail of higher values that extends to 626 ppm (Fig. 7). Using the input parameters from Kowalczyk et al. (2018) reduces the median estimate by ~60 ppm. 95% confidence intervals on the individual sample estimates vary in size, but mostly are limited to the interval 250–700 ppm. In some cases, however, the confidence intervals are strongly right-skewed and extend to over 1000 ppm (Fig. 7). Considering that most trees grew in elevated $pCO_2$ conditions of up to ~450 ppm, the model somewhat underestimates $pCO_2$.

The $C_3$ proxy, in both its $\Delta^{13}C$ and $\delta^{13}C$ iterations, generates $pCO_2$ estimates that for the most part underestimate ambient $pCO_2$ (lower quartile 304 ppm, median 352 ppm, upper quartile 434 ppm), but with a long right tail of higher values that extend to 711 ppm (Fig. 8). The 95% confidence intervals on the individual samples are wide and, in many cases, extend to over 1000 ppm, with a maximum upper confidence limit of 3481 ppm (Fig. 8).

### 3.5. Testing the influence of climate on reconstructed $pCO_2$

The relationships between the measured leaf parameters (i.e. stomatal measurements, $\delta^{13}C$) and the climatic variables feed through to the relationships between the $pCO_2$ proxy estimates and climate. The stomatal ratio and transfer function $pCO_2$ estimates are based on the stomatal index and as such show no clear relationship with temperature or precipitation (Figs. 9 and 10). The $pCO_2$ estimates from both the Franks model and the $C_3$ proxy are positively correlated to some extent with TAP and MAT because of the inclusion of $\delta^{13}C$ in both proxies (Figs. 9, 10 and S3), resulting in higher $pCO_2$ estimates in Köppen zone C versus zones B and D (Fig. 9 and S12). The effect of climate is most clear in the $C_3$ proxy, where both the mean and the variance of the $pCO_2$ estimates increase with TAP (Spearman's $rho = 0.55$, $p = 8.28 \times 10^{-13}$) and to a lesser extent with MAT (Spearman's $rho = 0.35$, $p = 2.02 \times 10^{-5}$). In the case of the Franks model, the relationship with the climate parameters is weaker (for TAP, Spearman's $rho = 0.35$, $p = 2.29 \times 10^{-5}$; for MAT, Spearman's $rho = 0.29$, $p = 4.96 \times 10^{-4}$). This is likely due to the inclusion of stomatal parameters in the Franks model (Fig. 11), which for the most part vary randomly with respect to the climatic variables (Fig. 4). This diffuses the control of precipitation acting through $\delta^{13}C$. As with the underlying measured parameters, there are no clear relationships between the $pCO_2$ proxy estimates and the population size of the sampled localities (Fig. S13), apart from the more negative $\delta^{13}C$ values in Shanghai and Tokyo propagating through to generally higher $pCO_2$ estimates for these cities.

When considering the $pCO_2$ estimates for Europe and China geographic subsets separately, patterns emerge that mirror those of the underlying measured parameters (Figs. S9, S10 and S14). While the stomatal ratio and transfer function approaches, which are based solely on the stomatal index, show no relationship with climate in either subset, the Franks and $C_3$ proxies, which incorporate $\delta^{13}C$, both show a relationship with MAT and TAP in the China subset that is stronger than in the dataset as a whole, but no clear relationship in the Europe subset (Fig. S14).

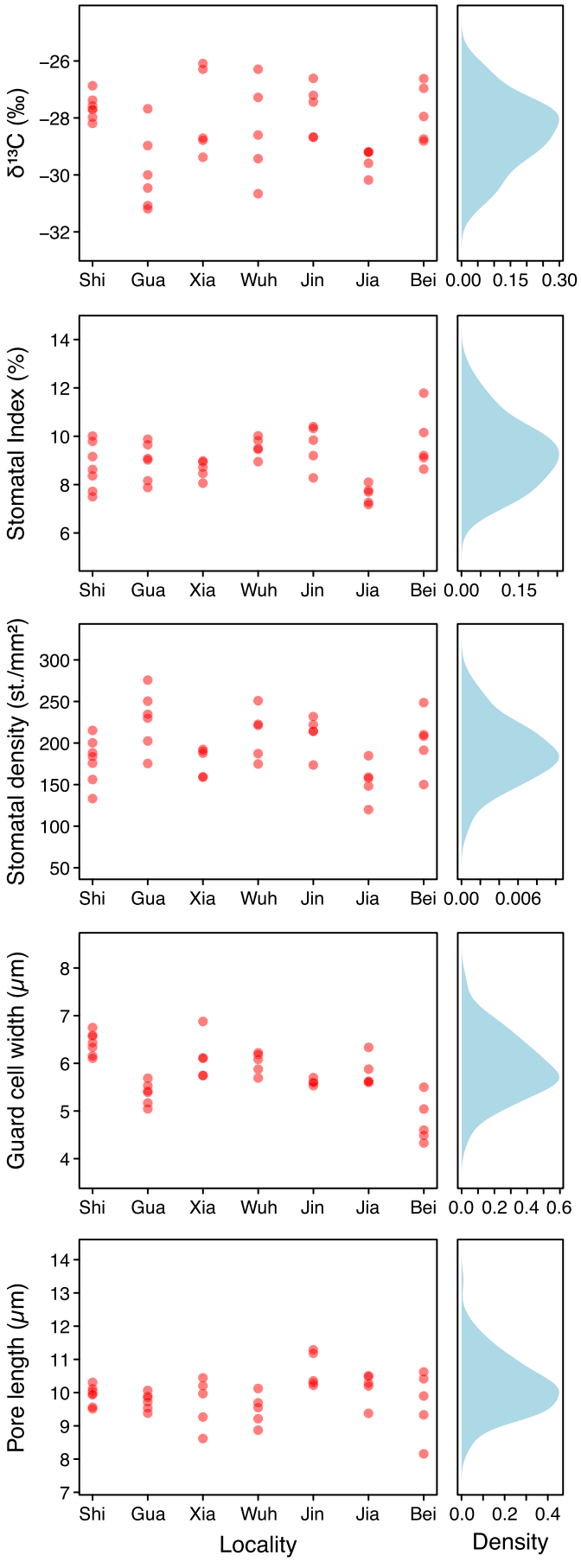


*(caption on next column)*

**Fig. 3.** Within-locality variability of parameter values (left) relative to entire dataset distributions (right, showing kernel density estimates). Each data point in the stripcharts represents one tree in each of the localities with five or more trees (Shi = Shihezi, Gua = Guangzhou, Xia = Xi'an, Wuh = Wuhan, Jin = Jinzhou, Jia = Jiangle, Bei = Beijing).

## 4. Discussion

The most important findings emerging from the data analysis are: i) that overall all the three stomatal proxy methods record $pCO_2$ reasonably well and similarly to each other; ii) that climate parameters, such as MAT and TAP, do not significantly influence stomata-based $pCO_2$ reconstructions; iii) and that there is a very large variability in all leaf traits, both within-tree, among-tree and within- and among localities. The main tested hypothesis that trees growing in warmer temperatures have higher leaf stomatal densities (and therefore record lower $pCO_2$) was rejected. The results support the assumption that stomatal parameters are principally controlled by $pCO_2$ and not influenced by climate (in contrast to the correlation between moisture availability and $\delta^{13}C$, affecting gas exchange models – see Section 4.1 below), further strengthening the robustness of the stomatal proxy for palaeo-$pCO_2$ reconstruction.

An important question is whether the variability observed from this large database of *G. biloba* leaves is natural or driven by some complex combination of environmental parameters not included in our data analysis. One possibility is that since most of the trees grow in urban and suburban environments, they might experience highly fluctuating $pCO_2$ which may 'confuse' the new leaves as they emerge. The best way to test this is to collect and analyze in the same manner *G. biloba* leaves from trees growing naturally in the wild in rural China, which is beyond the scope of this project. The unexpectedly large variation in key traits needs to be further tested, however, and considered when designing future palaeo-$pCO_2$ reconstruction studies. Building and testing large global databases of additional taxa important to palaeo-$pCO_2$ records, such as e.g. oaks, birches and conifers, would help answer the question 'what is the normal range of variability in key traits of a tree?'

### 4.1. Proxies in relation to climatic variability and implications for use

The results presented here show that higher temperatures do not downwardly bias plant-based $pCO_2$ proxies. The stomatal parameters show only weak and non-significant relationships with climate, which means that both the stomatal ratio and transfer function proxies, which solely rely on the stomatal index, can be used across intervals of climatic change without biases being imposed. However, the relationship between $\delta^{13}C$ and the climatic variables means that this effect needs to be considered when using the Franks and $C_3$ models to reconstruct palaeo-$pCO_2$. The relationship between $\delta^{13}C$ and TAP demonstrated by our data (Fig. 4) is consistent with previous studies (e.g. Kohn, 2010); the weaker relationship with MAT is likely to be because of the correlation between MAT and TAP in our data (Figs. S1 and 3). This is supported when considering geographic subsets of our data: in the European subset, where the correlation between MAT and TAP is weaker, there is no consistent relationship between $\delta^{13}C$ and MAT, whereas in the China subset, where the correlation between MAT and TAP is stronger, the strength of the relationship between $\delta^{13}C$ and MAT, and $\delta^{13}C$ and TAP, is similar (Figs. S9 and S10).

The impact of precipitation on the $C_3$ proxy is relatively stronger because this is entirely based on variations in $\delta^{13}C$; moisture availability effects therefore propagate straight through to the $pCO_2$ estimates. In the Franks model, the impact of precipitation is more diffuse: while $\delta^{13}C$ variations have a close relationship with the $pCO_2$ estimates, the inclusion of stomatal density, guard cell width and pore length in the model dampens the effect of moisture variability. The impact of $\delta^{13}C$ variations on $pCO_2$ estimates in these two proxies is also demonstrated in the two

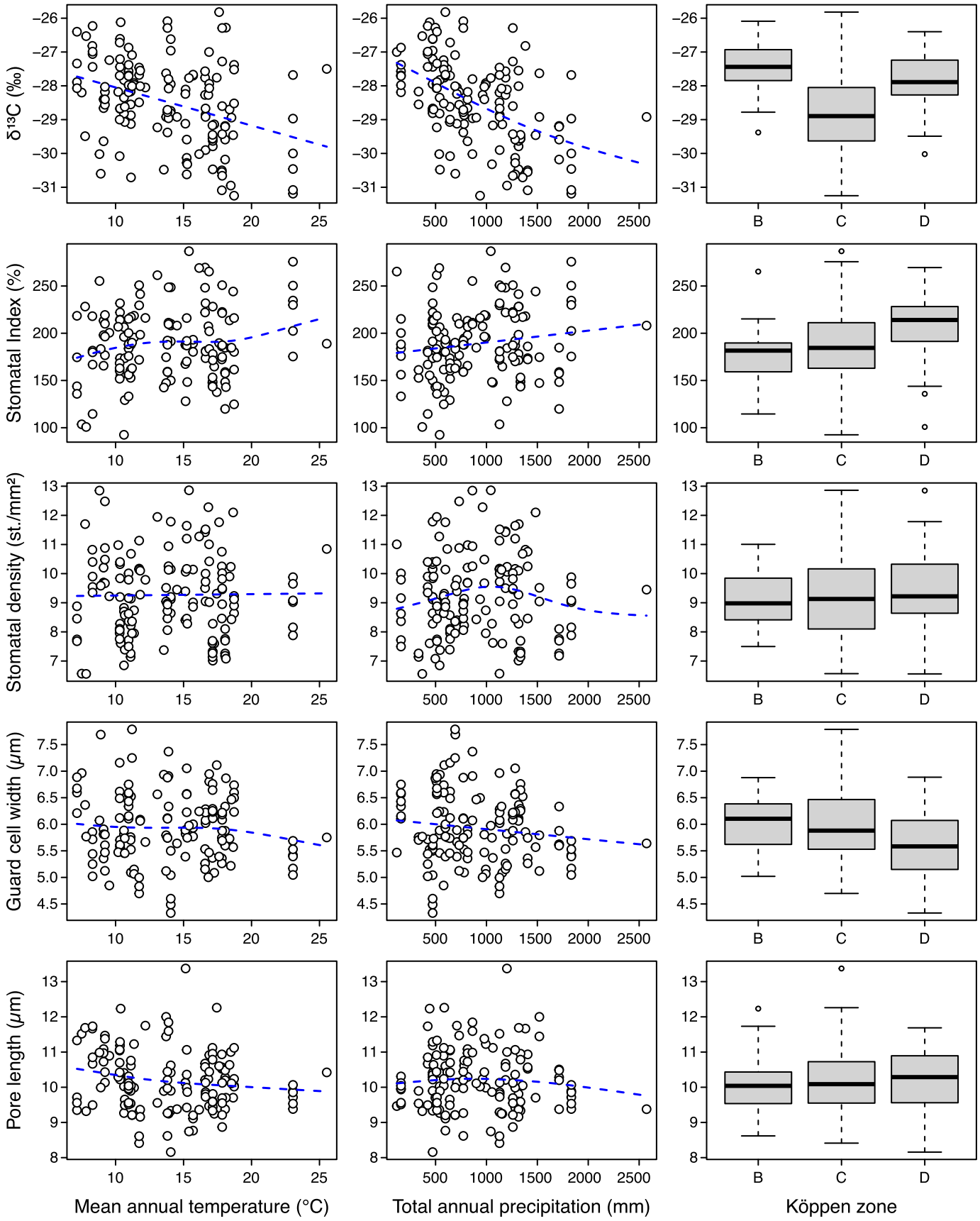


**Fig. 4.** Measured parameter values plotted against climate. Dashed blue lines show fitted additive model smoothers. Köppen zones included are B: Dry climates, C: Temperate/mesothermal climates and D: Continental/microthermal climates. (For interpretation of the references to colour in this figure legend, the reader is referred to the web version of this article.)

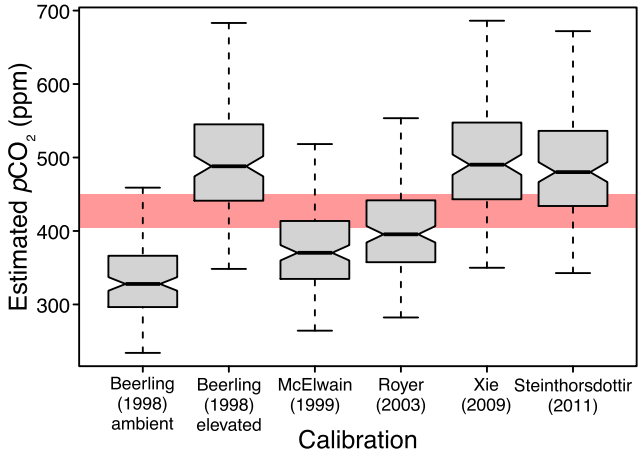


**Fig. 5.** $pCO_2$ estimates for different stomatal ratio calibrations. Shaded zone shows the 405 to 450 ppm interval (see Section 1.6 for details).

geographic subsets, with a narrower precipitation gradient and weaker relationship between precipitation and $\delta^{13}C$ in the European subset resulting in little or no influence of precipitation on the Franks and $C_3$ $pCO_2$ estimates, while in the China subset the approximately linear relationship between TAP and $\delta^{13}C$ results in a stronger imprint of TAP on estimated $pCO_2$ (Fig. S14).

The impact of variations in moisture availability on these proxies therefore needs to be considered when working on fossil material that extends over temporal or spatial gradients that encompass substantial climatic changes. However, working with taxonomically identified plant specimens may alleviate some of these issues because larger climatic changes are likely to force changes in plant composition, whereas if the composition remains relatively stable, and the same taxa are present throughout a sequence, it is more likely that any changes in moisture availability were more limited. This would however need to be confirmed with evidence from the depositional sedimentary context and ideally with independent climate proxies. Variations in moisture availability are likely to be more of a problem when the $C_3$ proxy is applied to sedimentary organic carbon which is derived from plants but without any clear taxonomic constraints (e.g. Schubert and Jahren, 2015; Cui et al., 2020); in these cases, changes in vegetation community composition cannot be used to infer environmental stability or change, and independent climatic information becomes more important.

### 4.2. $\delta^{13}C_{plant}$ and $\delta^{13}C_{air}$: Influence on $pCO_2$ reconstructions

Within our global dataset, there is wide variation in $\delta^{13}C_{plant}$, which is linked to variations in local climate, principally precipitation (Fig. 4). This variability then feeds through to influence $\Delta^{13}C$ providing a measure of plant water use efficiency (*WUE*). In our database calculations of $\Delta^{13}C$ have been achieved by using a constant value of $\delta^{13}C_{air}$ (−8.5‰). Over geological time, perturbations of the carbon cycle are recognised via changes in the carbon isotopes of measured substrates ($\delta^{13}C_{org}$ and $\delta^{13}C_{carb}$) as a reflection of a change in the isotopic composition of atmospheric $pCO_2$. This pattern (a negative carbon isotope excursion) has also been observed within the timeframe of the anthropogenic perturbation of the long-term carbon cycle. Applying either the $C_3$ or the Franks model to predict $pCO_2$ through carbon cycle perturbations when there is both a change in atmospheric $CO_2$ concentration and a change in the isotopic signature of the substrate is likely to introduce unaccounted for error in the predictions, because a component of the $pCO_2$ estimate will be linked to the isotopic signature of the air. Consequently, the unpicking of how changes in $\delta^{13}C_{air}$ influence $\delta^{13}C_{plant}$ when there is a change in $pCO_2$ may provide greater clarity on proxy/model intercomparisons. This issue is likely to be less impactful however when using the Franks model, as the stomatal parameters required in the model are likely to dampen the isotopic effect.

### 4.3. Variability and implications for sampling

Plants are phenotypically variable, and our ginkgo results demonstrate this variability both within and among trees and localities. Within-tree and within-locality variability is in many cases as substantial as among-tree variability (Fig. 3 and S4), and as noted above, most of the among-locality variability in the stomatal parameters is unexplained by climate, leading to a substantial amount of stochastic variation in these morphological traits. This has implications both in terms of sufficient sampling from extant plants for calibrating proxies, and for applying those proxies in the fossil record. The range of calibrations and input parameters that have been published for the different proxies is in part due to variations in sampling methods (e.g. updated stomatal and epidermal cell counting protocols in Barclay and Wing, 2016), but also because of the natural phenotypic variability that we have demonstrated here. Sufficient sampling is therefore important to gain representative

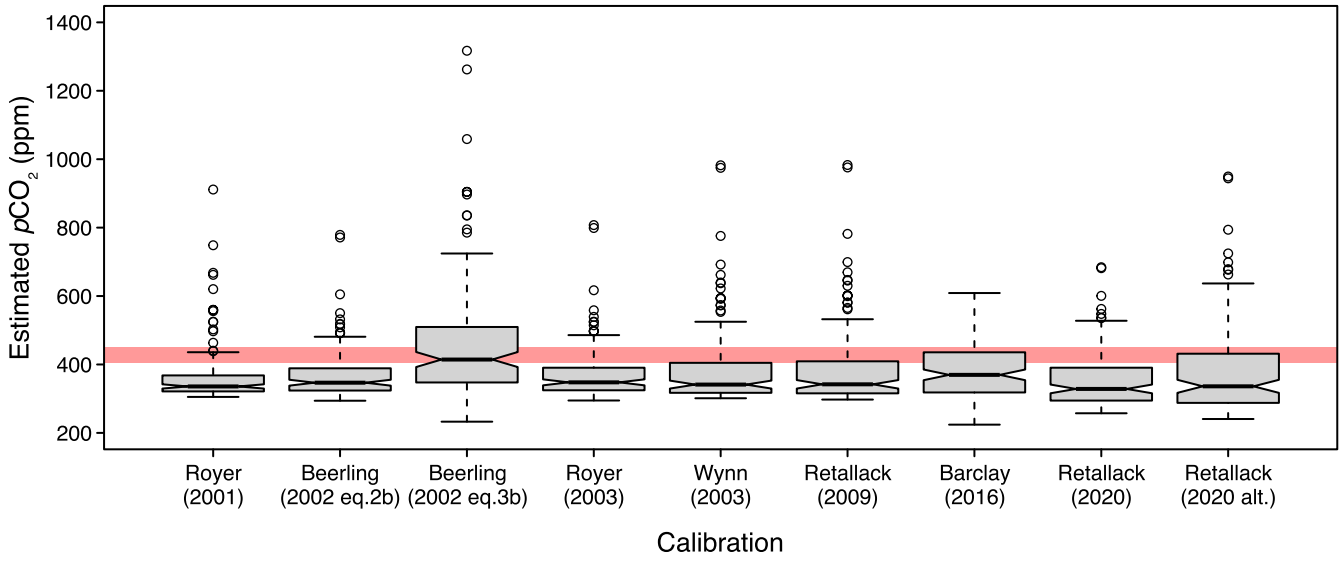


**Fig. 6.** $pCO_2$ estimates for different published transfer functions. Y axis is limited to 1500 ppm, excluding one anomalous value of 4141.6 ppm produced by the Royer et al. (2001) transfer function. Shaded zone shows the 405 to 450 ppm interval (see Section 1.6 for details).

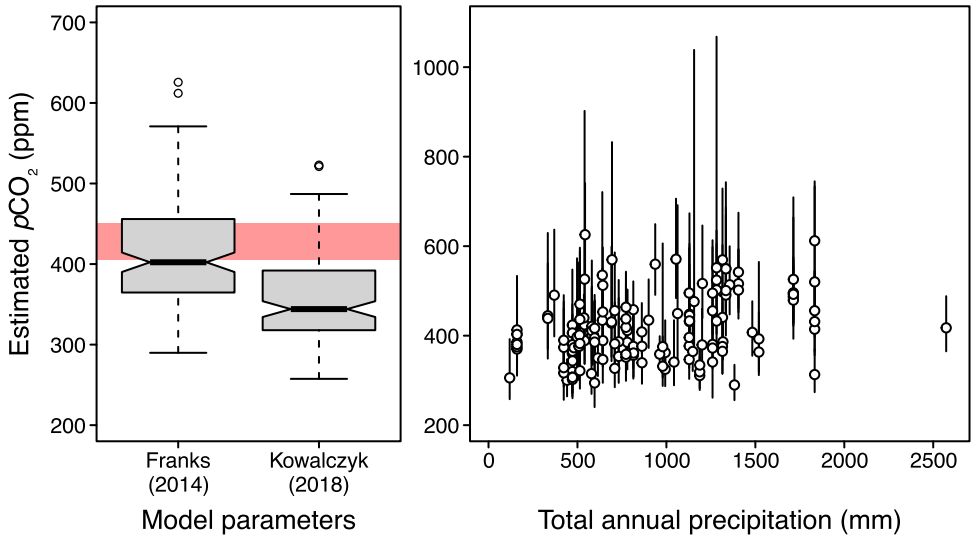


**Fig. 7.** $pCO_2$ estimates from the Franks model, using the input values provided by Franks et al. (2014) and Kowalczyk et al. (2018). Shaded zone shows the 405 to 450 ppm interval (see Section 1.6 for details). Right hand graph shows the estimates from the Franks et al. (2014) values plotted against total annual precipitation, with 95% confidence intervals derived from Monte Carlo resampling.

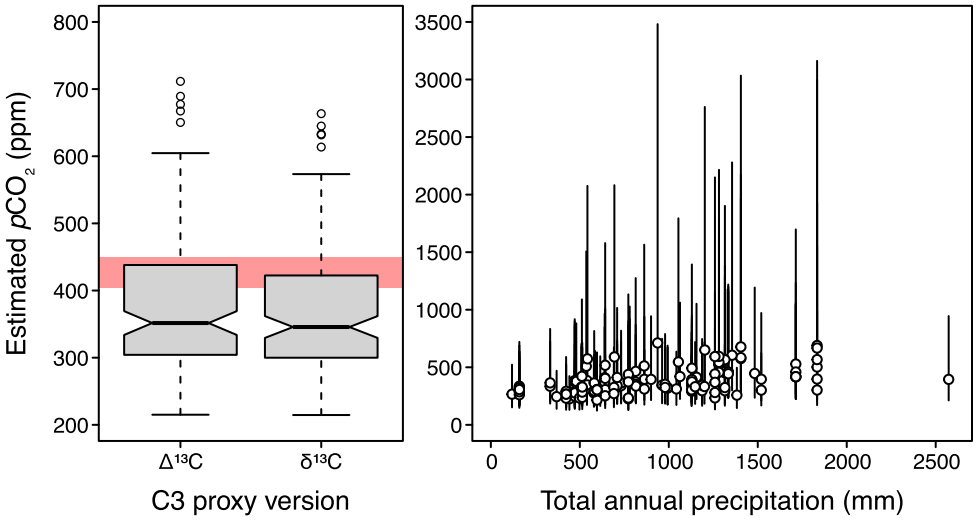


**Fig. 8.** $pCO_2$ estimates from the $C_3$ proxy, using both the $\Delta^{13}C$-based version (Schubert and Jahren, 2012, 2015; Cui et al., 2020) and the $\delta^{13}C$-based version (Cui et al., 2020). Shaded zone shows the 405 to 450 ppm interval (see Section 1.6 for details). Right hand graph shows the estimates from the $\Delta^{13}C$-based proxy plotted against total annual precipitation, with 95% confidence intervals derived from Monte Carlo resampling.

measurements.

For the stomatal ratio proxy this will involve collecting a sufficient number of leaves from a sufficient number of trees to gain a stable measure of the stomatal index at ambient $pCO_2$; we suggest that future implementations of this method with ginkgo fossils use the values from the global scale dataset presented here (SI mean = 9.28%, standard deviation = 1.60%, at 405–407 ppm global average $pCO_2$ during time of leaf collection). For transfer functions this will involve sufficiently dense sampling from across $pCO_2$ gradients to constrain the nonlinear functions used, with measurements at each individual time slice or $pCO_2$ level being just one realization of a wider distribution with potentially high variance. The Franks model relies on estimates of photosynthetic rate and $C_i/C_a$, and while the values given in Franks et al. (2014) converge on current ambient $pCO_2$ quite well, those given in Kowalczyk et al. (2018) reduce the estimates by ~60 ppm. Again, taking measurements from a sufficient number of trees is clearly necessary to gain a stable estimate to accurately reconstruct $pCO_2$ in fossil settings. We note that, in contrast to the stomatal ratio and transfer function approach, this more taxon-independent mechanistic gas-exchange model can be applied to fossil ginkgos, using measurements from modern *Ginkgo biloba*. Our results indicate that model should be used with the original input parameters and that the Franks model will reproduce palaeo-$pCO_2$ using fossil ginkgos well.

Careful consideration of sufficient sampling therefore needs to be built into study designs, with the awareness that how much sampling is sufficient is likely to vary according to taxon, the parameter being measured and possibly ambient growth conditions. Global scale datasets for other taxa, to help determine what is 'normal' for these, are also recommended, as well as dedicated sampling within and among trees within one locality, to better understand how trait variability is partitioned and how this variability is represented in fossil deposits, as well as how sampling should be focused in extant and fossil studies. For studies in the fossil record, where sampling extent is often constrained by outcrop and material availability, multi-taxon, multi-method palaeo-

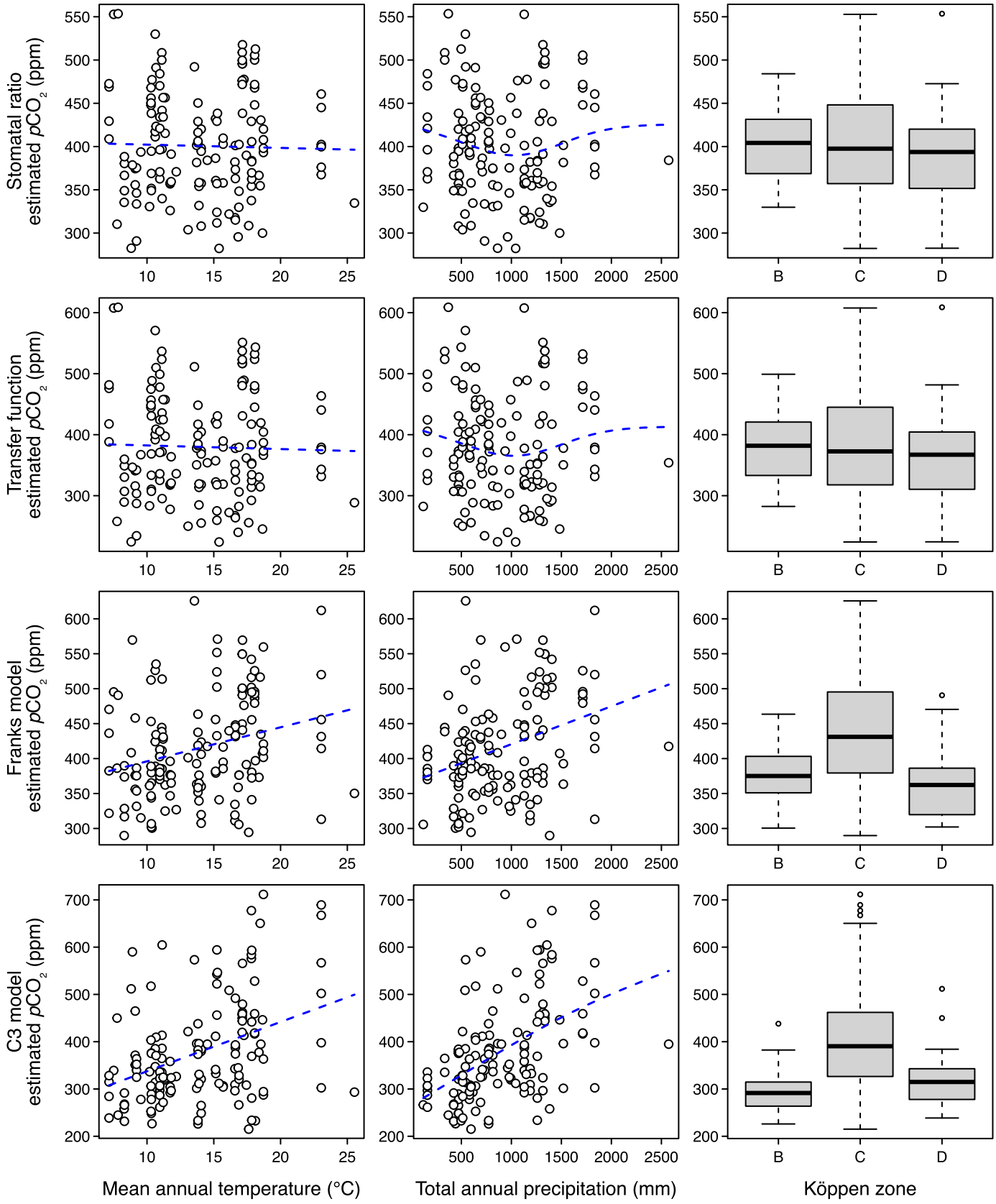


**Fig. 9.** $pCO_2$ estimates from the four proxies plotted against climatic parameters. The stomatal ratio estimates are from the Royer (2003) calibration, the transfer function estimates are from the Barclay and Wing (2016) function, the Franks model estimates use the Franks et al. (2014) input parameters, and the C3 model estimates are from the $\Delta^{13}C$-based version. Dashed blue lines are fitted additive model smoothers.

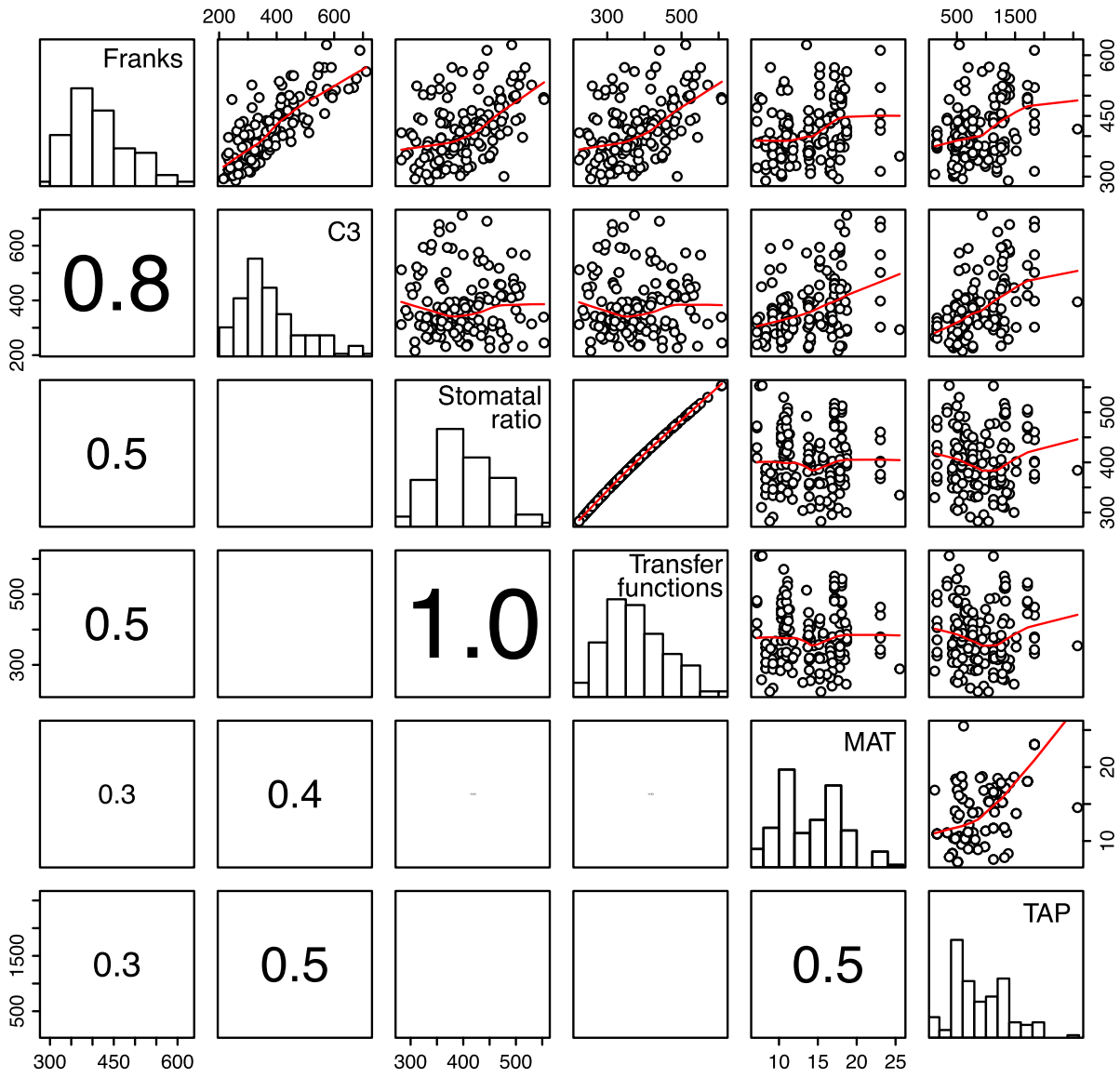


**Fig. 10.** Pairs plot showing the relationship between the $pCO_2$ proxy estimates and climate. The calibrations and parameters used for each proxy are the same as in Fig. 9. Red lines show loess smoothers, the histograms along the diagonal show the distribution of each set of values, and the lower half of the figure gives correlation coefficients (Pearson's *r*) for each pair of proxy estimates or climate variables. (For interpretation of the references to colour in this figure legend, the reader is referred to the web version of this article.)

$pCO_2$ reconstructions (e.g. Steinthorsdottir et al., 2021b) are likely to be beneficial to help average out the natural variation encompassed in measurements and calibrations.

### 4.4. Potential implications for Earth's climate sensitivity and future warming

The results presented here show that the stomatal proxy methods recorded global average $pCO_2$ reasonably well and in broad agreement with one another, with no consistent influence of climate on stomatal parameters that leads to either systematic under- or over-estimation of reconstructed $pCO_2$. Assuming that this was also the case in the past, stomatal proxies are correctly recording $pCO_2$ and climate sensitivity was instead significantly elevated during MCO and other Cenozoic warm episodes, leading to highly elevated temperatures at moderate $pCO_2$. Elevated climate sensitivity in the Cenozoic, especially during warmer relative to colder intervals, has repeatedly been suggested, based on simulations and comparisons to proxy records (e.g. Goldner et al., 2014; Anagnostou et al., 2016; Shaffer et al., 2016; Wolfe et al., 2017; Cramwinckel et al., 2018; Steinthorsdottir et al., 2019b; Inglis et al., 2020). Modern climate sensitivity may be in a relatively depressed state in the context of the geological record, due to low rate of feedbacks owing to the low $pCO_2$ baseline, presence of ice sheets and the relatively small ocean area in the modern geographical configuration (Farnsworth et al., 2019). The climate system today is likely out of equilibrium with radiative forcing due to the fast pace of emissions (von der Heydt et al., 2016), emphasizing the importance of state dependence for climate sensitivity. Strong evidence thus suggests that climate sensitivity increases under high $pCO_2$ conditions, due to the feedback temperature dependency and is not same for different baseline $pCO_2$ (Shaffer et al., 2016; Bloch-Johnson et al., 2015a; 2021; Wong et al., 2021). Some climate system models suggest that climate sensitivity increases with MAT, driven in particular by a combination of water vapour and cloud feedback, despite loss of albedo (Caballero and Huber, 2013; Popp et al., 2016; Bloch-Johnson et al., 2021), although other factors such as changes in solar luminosity, paleogeography and ocean circulation may also play a significant role (von der Heydt et al., 2016; Farnsworth et al., 2019). Greater climate sensitivity may then amplify the ongoing

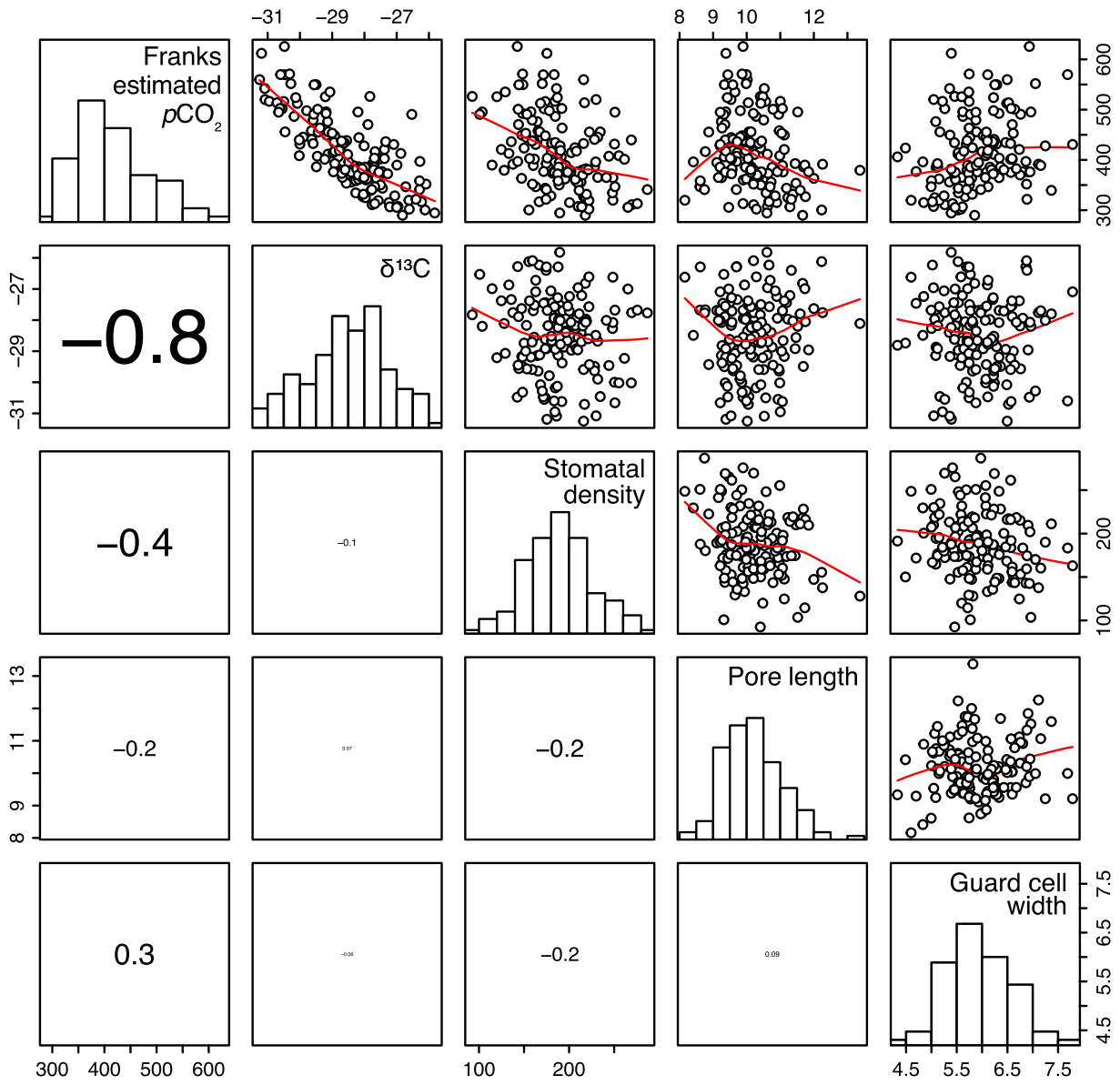


**Fig. 11.** Pairs plot showing the relationship between the Franks model $pCO_2$ estimates and the measured input parameters. See Fig. 10 caption for an explanation of the plot.

warming – the more the climate warms, the more it needs to warm to balance a further increase in $pCO_2$, because the system becomes less effective at rebalancing energy flows with increased warming (Bloch--Johnson et al., 2015b; 2021). Given that the plethora of MCO and other Cenozoic warm episode proxy records record moderately elevated $pCO_2$ during intervals of highly elevated temperatures (see Section 1.1), and the evidence presented here that living (and presumably fossil) plants do not underestimate $pCO_2$ under these conditions, the hypothesis of elevated climate sensitivity under elevated temperatures is supported. With no signs yet of decreasing global emissions, we are fast approaching predicted MCO-level $pCO_2$. It is therefore urgent to improve our knowledge of the Earth system's climate sensitivity, in order to understand whether relatively moderate, near-modern levels of $pCO_2$ may result in a devastating temperature increase sooner than presently predicted.

## 5. Conclusions

Past episodes of rapid climate change from the Cenozoic are the best future climate analogues, since the present warming is unprecedented in instrumental records. However, reconstructed $pCO_2$ is too low during some of these episodes to reproduce in climate models the temperatures observed. Either climate sensitivity was elevated in the past, models are currently missing important positive forcings, or proxies underestimate $pCO_2$ due to additional environmental factors. Here we tested the impact of climate on the stomatal proxy for $pCO_2$ reconstruction. We used a large global leaf database of the important proxy species *G. biloba*, comparing reconstructions based on three stomatal proxy methods and the $C_3$ proxy. Data analysis suggests that neither high temperatures nor other climate parameters result in significant underpredictions of $pCO_2$ using the stomatal proxy, but that natural variability in key traits is very high. The lack of climatic control on stomatal parameters strengthens the reliability of the stomatal proxy for $pCO_2$ reconstructions and suggests that climate sensitivity was elevated during warm episodes in the Cenozoic.

## Data availability

All data and R code are provided in the supplementary information and in the Bolin Centre for Climate Research (Stockholm University) database [doi to come].

## Declaration of Competing Interest

The authors declare that they have no known competing financial interests or personal relationships that could have appeared to influence the work reported in this paper.

## Acknowledgements

We sincerely thank the numerous citizen scientists, friends and colleagues around the world listed in Table S2, who enabled this project by collecting and shipping the ginkgo leaves, in particular Liping Liu and Yongdong Wang, who organized the bulk of the China collection. We thank Anna Lindström and Khaled Abou, Swedish Museum of Natural History, for help with data collection. Tammo Reichgelt kindly provided the locality map used in the graphical abstract. We are grateful to Matt Huber, Rodrigo Caballero, Jenny McElwain, Vivi Vajda, and numerous additional colleagues for discussions that helped improve this project, and to the reviewers who helped improve the manuscript. M.S. would like to acknowledge funding from the Swedish Research Council, who supported this research with grant nr. NT7-2016 04905, and from the Bolin Centre for Climate Research, Stockholm University. B.H.L acknowledges funding from the NERC (grant nr. NE/R001324/1 and NE/T00392/1). P.E.J. is funded by the Deutsche Forschungsgemeinschaft (DFG, German Research Foundation) project nr. 443701866. T.S. is supported by funding from the Carl Trygger Foundation postdoctoral grant (contract CTS 18:167).

## Appendix A. Supplementary data

Supplementary data to this article can be found online at https://doi.org/10.1016/j.gloplacha.2022.103786.

## References

Anagnostou, E., John, E.H., Edgar, K.M., Foster, G.L., Ridgwell, A., Inglis, G.N., Pancost, R.D., Lunt, D.J., Pearson, P.N., 2016. Changing atmospheric $CO_2$ concentration was the primary driver of early Cenozoic climate. Nature 533, 308–384. https://doi.org/10.1038/nature17423.

Bacon, K.L., Belcher, C.M., Haworth, M., McElwain, J.C., 2013. Increased atmospheric $SO_2$ detected from changes in leaf physiognomy across the Triassic-Jurassic boundary interval of East Greenland. PLoS One 8 (4), e60614. https://doi.org/10.1371/journal.pone.0060614.

Bainian Sun, David Dilcher, L., David Beerling, J., Chengjun Zhang, Defei Yan, Elizabeth Kowalsk, 2003. Variation inGinkgo bilobaL. leaf characters across aclimatic gradient in China, 100. PNAS, pp. 7141–7146.

Barclay, R.S., Wing, S.L., 2016. Improving the Ginkgo $CO_2$ barometer: implications for the early Cenozoic atmosphere. Earth Planet. Sci. Lett. 439, 158–171.

Beerling, D.J., Andrew Fox, Clive Anderson, W., 2009. Quantitative uncertainty analyses of ancient atmospheric CO2 estimates from fossil leaves. Am. J. Sci. 309 (9), 775–787. https://doi.org/10.2475/09.2009.01.

Beerling, D.J., Chaloner, W.G., 1993. The impact of atmospheric $CO_2$ and temperature changes on stomatal density: observations from *Quercus robur* Lammas leaves. Ann. Bot. 71, 231–235.

Beerling, D.J., Royer, D.L., 2002. Reading a $CO_2$ signal from fossil stomata. New Phytol. 153, 387–397.

Beerling, D.J., Royer, D.L., 2011. Convergent Cenozoic $CO_2$ history. Nat. Geosci. 4, 418–420. https://doi.org/10.1038/ngeo1186.

Beerling, D.J., McElwain, J.C., Osborne, C.P., 1998. Stomatal responses of the "living fossil" *Ginkgo biloba* L. to changes in atmospheric $CO_2$ concentrations. J. Exp. Bot. 49 (326), 1603–1607.

Beerling, D.J., Lomax, B.H., Royer, D.L., Upchurch, G.R., Kump, L.R., 2002. An atmospheric $pCO_2$ reconstruction across the Cretaceous–Tertiary boundary from leaf megafossils. Proc. Natl. Acad. Sci. U. S. A. 99, 7836–7840.

Bivand, R., Keitt, T., Rowlingson, B., 2021. rgdal: bindings for the 'geospatial' data abstraction library. In: R Package Version 1.5–23. https://CRAN.R-project.org/package=rgdal.

Bloch-Johnson, J., Pierrehumbert, R.T., Abbot, D.S., 2015a. Feedback temperature dependence determines the risk of high warming. Geophys. Res. Lett. 42, 4973–4980. https://doi.org/10.1002/2015GL064240.

Bloch-Johnson, J., Rugenstein, M., Stolpe, M.B., Rohrschneider, T., Zheng, Y., Gregory, J. M., 2015b. Climate sensitivity increases under higher $CO_2$ levels due to feedback temperature dependence. Geophys. Res. Lett. 48, e2020GL089074 https://doi.org/10.1029/2020GL089074.

Bloch-Johnson, J., Rugenstein, M., Stolpe, M.B., Rohrschneider, T., Zheng, Y., Gregory, J. M., 2021. Climate sensitivity increases under higher CO2 levels due to feedback temperature dependence. Geophys. Res. Lett. 48 https://doi.org/10.1029/2020GL089074 e2020GL089074.

Burke, K.D., Williams, J.W., Chandler, M.A., Haywood, A.M., Lunt, D.J., Otto-Bliesner, B. L., 2018. Pliocene and Eocene provide best analogs for near-future climates. Proc. Natl. Acad. Sci. U. S. A. 115, 13288–13293.

Caballero, R., Huber, M., 2013. State-dependent climate sensitivity in past warm climates and its implications for future climate projection. Proc. Natl. Acad. Sci. U. S. A. 110, 14162–14167.

Chen, L.-Q., Cheng-Sen, L., Chaloner, W.G., Beerling, D.J., Sun, Q.-G., Collinson, M.E., Mitchell, P.L., 2001. Assessing the potential for the stomatal characters of extant and fossil *Ginkgo* leaves to signal atmospheric $CO_2$ change. Am. J. Bot. 88, 1309–1315.

Cramwinckel, M.J., Huber, M., Kocken, I.J., Agnini, C., Bijl, P.K., Bohaty, S.M., et al., 2018. Synchronous tropical and polar temperature evolution in the Eocene. Nature 559, 382–386. https://doi.org/10.1038/s41586-018-0272-2.

Crane, P.R., 2013. Ginkgo: The Tree that Time Forgot. Yale University Press, New Haven.

Cui, Y., Schubert, B.A., Jahren, A.H., 2020. A 23 m.y. record of low atmospheric $CO_2$. Geology 48, 888–892. https://doi.org/10.1130/G47681.1.

Diefendorf, A.F., Freeman, K.H., Wing, S.L., Currano, E.D., Mueller, K.E., 2015. Paleogene plants fractionated carbon isotopes similar to modern plants. Earth Planet. Sci. Lett. 429, 33–44.

Farnsworth, A., Lunt, D.J., O'Brien, C.L., Foster, G.L., Inglis, G.N., Markwick, P., et al., 2019. Climate sensitivity on geological timescales controlled by nonlinear feedbacks and ocean circulation. Geophys. Res. Lett. 46, 9880–9889. https://doi.org/10.1029/2019GL083574.

Foster, G.L., Lear, C.H., Rae, J.W.B., 2012. The evolution of $pCO_2$, ice volume and climate during the middle Miocene. Earth Planet. Sci. Lett. 341, 243–254.

Foster, G.L., Royer, D.L., Lunt, D.J., 2017. Future climate forcing potentially without precedent in the last 420 million years. Nat. Commun. 8, 14845.

Franks, P.J., Royer, D.L., Beerling, D.J., Van de Water, P.K., Cantrill, D.J., Barbour, M.M., Berry, J.A., 2014. New constraints on atmospheric $CO_2$ concentration for the Phanerozoic. Geophys. Res. Lett. 41, 4685–4694. https://doi.org/10.1002/2014GL060457.

Friis, E.M., Crane, P.R., Pedersen, K.R., 2011. Early Flowers and Angiosperm Evolution. Cambridge University Press, p. 600.

Frommer, W.B., 2010. $CO_2$mmon sense. Science 327, 275–276.

George, K., Ziska, L.H., Bunce, J.A., Quebedeaux, B., 2007. Elevated atmospheric $CO_2$ concentration and temperature across an urban-rural transect. Atmos. Environ. 41, 7654–7665.

Goldner, A., Herold, N., Huber, M., 2014. The challenge of simulating the warmth of the mid-Miocene climatic optimum in CESM1. Clim. Past 10 (2), 523–536.

Gratani, L., Varone, L., 2005. Daily and seasonal variation of $CO_2$ in the city of Rome in relationship with the traffic volume. Atmos. Environ. 39, 2619–2624.

Graven, H., Keeling, R.F., Rogelj, J., 2020. Changes to carbon isotopes in Atmospheric $CO_2$ over the industrial era and into the future. Glob. Biogeochem. Cycles 34, e2019GB006170.

Gray, J.E., Holroyd, G.H., van der Lee, F.M., Bahrami, A.R., Sijmons, P.C., Woodward, F. I., Schuch, W., Hetherington, A.M., 2000. The HIC signalling pathway links $CO_2$ perception to stomatal development. Nature 408, 713–716.

Greenop, R., Foster, G.L., Wilson, P.A., Lear, C.H., 2014. Middle-Miocene climate instability associated with high-amplitude $CO_2$ variability. Paleoceanography 29, 845–853.

Grein, M., Oehm, C., Konrad, W., Utescher, T., Kunzmann, L., Roth-Nebelsick, A., 2013. Atmospheric $CO_2$ from the late Oligocene to early Miocene based on photosynthesis data and fossil leaf characteristics. Palaeogeogr. Palaeoclimatol. Palaeoecol. 374, 41–51.

Guan, R., Zhao, Y., Zhang, H., Fan, G., Liu, X., Zhou, W., et al., 2016. Draft genome of the living fossil *Ginkgo biloba*. GigaScience 5, 49.

Haiduc, I., Beldean-Galea, M.S., 2011. Variation of greenhouse gases in urban areas – case study: $CO_2$, CO and $CH_4$ in three Romanian cities. IntechOpen.

Hansen, J., Sato, M., Russell, G., Kharecha, P., 2013. Climate sensitivity, sea level and atmospheric carbon dioxide. Philos. *T. Roy*. Soc. A 371, 20120294. https://doi.org/10.1098/rsta.2012.0294.

Hare, V.J., Lavergne, A., 2021. Differences in carbon isotope discrimination between angiosperm and gymnosperm woody plants, and their geological significance. Geochim. Cosmochim. Acta 300, 215–230.

Harris, I., Osborn, T.J., Jones, P., Lister, D., 2020. Version 4 of the CRU TS monthly high-resolution gridded multivariate climate dataset. Sci. Data 7, 109. https://doi.org/10.1038/s41597-020-0453-3.

Hausfather, Z., 2018. Analysis: Why the IPCC 1.5C Report Expanded the Carbon Budget. CarbonBrief. https://www.carbonbrief.org/analysis-how-much-carbon-budget-is-left-to-limit-global-warming-to-1-5c.

Haworth, M., Hesselbo, S.P., McElwain, J.C., Robinson, S.A., Brunt, J.W., 2005. Mid-cretaceous $pCO_2$ based on stomata of the extinct conifer *Pseudofrenelopsis* (Cheirolepidiaceae). Geology 33, 749–752.

Haworth, M., Heath, J., McElwain, J.C., 2010. Differences in the response sensitivity of stomatal index to atmospheric $CO_2$ among four genera of Cupressaceae conifers. Ann. Bot. 105, 411–418.

Haywood, A., Dowsett, H., Dolan, A., 2016. Integrating geological archives and climate models for the mid-Pliocene warm period. Nat. Commun. 7, 10646. https://doi.org/10.1038/ncomms10646.
Hijmans, R.J., 2021. Raster: Geographic Data Analysis and Modeling. R Package Version 3.4-13. https://CRAN.R-project.org/package=raster.
Hincke, A.J.C., Broere, T., Kürschner, W.M., Donders, T.H., Wagner-Cremer, F., 2016. Multi-year leaf-level response to sub-ambient and elevated experimental $CO_2$ in *Betula nana*. PLOSone, 11(6): e0157400.
Huber, M., 2013. A sensitivity to history. Nat. Geosci. 6, 15–16.
Huber, M., Beyerle, U., Knutti, R., 2014. Estimating climate sensitivity and future temperature in the presence of natural climate variability. Geophys. Res. Lett. 41, 2086–2092.
Idso, C.D., Idso, S.B., Balling, R.C., 1998. The urban $CO_2$ dome of Phoenix, Arizona. Phys. Geogr. 19, 95–108.
Idso, C.D., Idso, S.B., Balling, R.C., 2001. An intensive two-week study of an urban $CO_2$ dome. Atmos. Environ. 35, 995–1000.
Idso, S.B., Idso, C.D., Balling, R.C., 2002. Seasonal and diurnal variations of near-surface atmospheric $CO_2$ concentrations within a residential sector of the urban $CO_2$ dome of Phoenix, AZ, USA. Atmos. Environ. 36, 1655–1660.
Imasu, R., Tanabe, Y., 2018. Diurnal and seasonal variations of carbon dioxide ($CO_2$) concentration in urban, suburban, and rural areas around Tokyo. Atmosphere 9, 367. https://doi.org/10.3390/atmos9100367.
Inglis, G.N., Bragg, F., Burls, N., Evans, D., Foster, G.L., Huber, M., Lunt, D.J., et al., 2020. Global mean surface temperature and climate sensitivity of the EECO, PETM and latest paleocene. Clim. Past. https://doi.org/10.5194/cp-2019-167.
IPCC, 2021. Climate change 2021: the physical science basis. In: Masson-Delmotte, V., Zhai, P., Pirani, A., Connors, S.L., Péan, C., Berger, S., Caud, N., Chen, Y., Goldfarb, L., Gomis, M.I., Huang, M., Leitzell, K., Lonnoy, E., Matthews, J.B.R., Maycock, T.K., Waterfield, T., Yelekçi, O., Yu, R., Zhou, B. (Eds.), Contribution of Working Group I to the Sixth Assessment Report of the Intergovernmental Panel on Climate Change. Cambridge University Press (In Press).
Jardine, P.E., Lomax, B.H., 2021. A 23 m.y. record of low atmospheric $CO_2$: COMMENT. Geology 49, e523. https://doi.org/10.1130/G48596C.1.
Keeling, C.D., Piper, S.C., Whorf, T.P., Keeling, R., 2010. Evolution of natural and anthropogenic fluxes of atmospheric $CO_2$ from 1957 to 2003. Tellus Ser. B Chem. Phys. Meteorol. 63, 1–22. https://doi.org/10.1111/j.1600-0889.2010.00507.x.
Kim, S., 2015. ppcor: Partial and Semi-Partial (Part) Correlation. R Package Version 1.1. https://CRAN.R-project.org/package=ppcor.
Knutti, R., Rugenstein, M.A.A., Hegerl, G.C., 2017. Beyond equilibrium climate sensitivity. Nat. Geosci. 10, 727–736.
Kohn, M.J., 2010. Carbon isotope compositions of terrestrial C3 plants as indicators of (paleo)ecology and (paleo)climate. Proc. Natl. Acad. Sci. U. S. A. 107, 19691–19695. https://doi.org/10.1073/pnas.1004933107.
Konrad, W., Katul, G., Roth-Nebelsick, A., Grein, M., 2017. A reduced order model to analytically infer atmospheric $CO_2$ concentration from stomatal and climate data. Adv. Water Resour. 104, 145–157.
Konrad, W., Royer, D., Franks, P.J., Roth-Nebelsick, A., 2020. Quantitative critique of leaf-based paleo-$CO_2$ proxies: Consequences for their reliability and applicability. Geol. J. 1–17.
Kottek, M., Grieser, J., Beck, C., Rudolf, B., Rubel, F., 2006. World Map of the Köppen-Geiger climate classification updated. Meteorol. Z. 15, 259–263. https://doi.org/10.1127/0941-2948/2006/0130.
Kouwenberg, L.R., McElwain, J.C., Kürschner, W.M., Wagner, F., Beerling, D.J., Mayle, F. E., Visscher, H., 2003. Stomatal frequency adjustment of four conifer species to historical changes in atmospheric $CO_2$. Am. J. Bot. 90, 610–619.
Kowalczyk, J.B., Royer, D.L., Miller, I.M., Anderson, C.W., Beerling, D.J., Franks, P.J., et al., 2018. Multiple proxy estimates of atmospheric $CO_2$ from an early Paleocene rainforest. Paleoceanogr. Paleoclimatol. 33, 1427–1438. https://doi.org/10.1029/2018PA003356.
Kürschner, W.M., van der Burgh, J., Visscher, H., Dilcher, D., 1996. Oakleaves as biosensors of late Neogene and early Pleistocene paleoatmosperic $CO_2$ concentrations. Mar. Micropaleontol. 27, 213–299.
Kürschner, W.M., Kvaček, Z., Dilcher, D.L., 2008. The impact of Miocene atmospheric carbon dioxide fluctuations on climate and the evolution of terrestrial ecosystems. Proc. Natl. Acad. Sci. U. S. A. 105, 449–453.
Lake, J.A., Quick, W.P., Beerling, D.J., Woodward, F.I., 2001. Plant development - Signals from mature to new leaves. Nature 411, 154.
Lamigueiro, O.P., Hijmans, R., 2021. rasterVis. R Package Version 0.51.0. https://oscarperpinan.github.io/rastervis/.
Lomax, B.H., Lake, J.A., Leng, M.J., Jardine, P.E., 2019. An experimental evaluation of the use of d13C as a proxy for palaeoatmospheric CO2. Geochim. Cosmochim. Acta 247, 162–174.
Loveys, B, Scheurwater, I, Pons, T, Fitter, A, Atkin, O, 2002. Growth temperature influences the underlying components of relative growth rate: an investigation using inherently fast- and slow-growing plant species. Plant, Cell & Environment 25, 975–988.
Lunt, D.J., Haywood, A.M., Schmidt, G.A., Salzmann, U., Valdes, P.J., Dowsett, H.J., 2010. Earth system sensitivity inferred from Pliocene modelling and data. Nat. Geosci. 3, 60–64.
Luomala, E., Laitinen, K., Sutinen, S., Kellomäki, S., Vapaavuori, E., 2005. Stomatal density, anatomy and nutrient concentrations of Scots pine needles are affected by elevated CO2 and temperature. Plant, Cell & Environment 28, 733–749.
Manley, G., 1958. On the frequency of snowfall in metropolitan England. Q. J. R. Meteorol. Soc. 8, 70–72.
Mays, C., Steinthorsdottir, M., Stillwell, J.D., 2015. Climatic implications of *Ginkgoites waarensis* Douglas emend. From the south polar Tupuangi flora, late cretaceous (Cenomanian), Chatham Islands. Palaeogeogr. Palaeoclimatol. Palaeoecol. 438, 308–326.
McElwain, J.C., 1998. Do fossil plants signal palaeoatmospheric carbon dioxide concentration in the geological past? Philos. Trans. R. Soc. Lond. B 353, 83–96.
McElwain, J.C., Steinthorsdottir, M., 2017. Palaeoecology, ploidy, palaeoatmospheric composition and developmental biology: a review of the multiple uses of fossil stomata. Plant Physiol. 174, 650–664.
McElwain, J.C., Beerling, D.J., Woodward, F.I., 1999. Fossil plants and global warming at the Triassic–Jurassic boundary. Science 285, 1386–1390.
McElwain, J.C., Montañez, I.P., White, J.D., Wilson, J.P., Yiotis, C., 2016. Was atmospheric $CO_2$ capped at 1000 ppm over the past 300 million years? Palaeogeogr. Palaeoclimatol. Palaeoecol. 441, 653–658.
Montañez, I.P., McElwain, J.C., Poulsen, C.J., White, J.D., DiMichele, W.A., Wilson, J.P., Griggs, G., Hren, M.T., 2016. Climate, $pCO_2$ and terrestrial carbon cycle linkages during late Palaeozoic glacial-interglacial cycles. Nat. Geosci. 9, 824–828.
Moriwaki, R., Kanda, M., Nitta, H., 2006. Carbon dioxide build-up within a suburban canopy layer in winter night. Atmos. Environ. 40, 1394–1407.
Pagani, M., Liu, Z., Larivieri, J., Ravelo, A.C., 2010. High Earth-system climate sensitivity determined from Pliocene carbon dioxide concentrations. Nat. Geosci. 3, 27–30. https://doi.org/10.1038/ngeo724.
Peppe, D.J., Royer, D.L., Cariglino, B., Oliver, S.Y., Newman, S., et al., 2011. Sensitivity of leaf size and shape to climate: global patterns and paleoclimatic applications. New Phytol. 190, 724–739. https://doi.org/10.1111/j.1469-8137.2010.03615.x.
Pigliautile, I., Marseglia, G., Pisello, A.L., 2020. Investigation of $CO_2$ variation and mapping through wearable sensing techniques for measuring pedestrians' exposure in urban areas. Sustainability 12, 3936. https://doi.org/10.3390/su12093936.
Popp, M., Schmidt, H., Marotzke, J., 2016. Transition to a moist greenhouse with $CO_2$ and solar forcing. Nat. Commun. 7 (10), 627. https://doi.org/10.1038/ncomms10627.
R Core Team, 2021. R: A Language and Environment for Statistical Computing. R Foundation for Statistical Computing, Vienna, Austria. https://www.R-project.org/.
Reddy, K., Robana, R., Hodges, H.F., Liu, X, McKinion, J.M., 1998. Interactions of CO2 enrichment and temperature on cotton growth and leaf characteristics. Environmental and Experimental Botany 39, 117–129.
Retallack, G.J., 2001. A 300-million year record of atmospheric carbon dioxide from fossil plant cuticles. Nature 411, 287–290.
Retallack, G.J., 2002. Carbon dioxide and climate over the past 300 Myr. Philos. Trans. R. Soc. Lond. Ser. A Math. Phys. Eng. Sci. 360, 659–673.
Retallack, G.J., 2009. Greenhouse crises of the past 300 million years. Geol. Soc. Am. Bull. 121, 1441–1455.
Retallack, G.J., Conde, G.D., 2020. Deep time perspective on rising atmospheric $CO_2$. Glob. Planet. Chang. 189, 103177.
Royer, D.L., 2003. Estimating latest cretaceous and Tertiary atmospheric $CO_2$ from stomatal indices. In: Wing, S.L., Gingerich, P.D., Schmitz, B., Thomas, E. (Eds.), Causes and Consequences of Globally Warm Climates in the Early Paleogene, 369. Geol. Soc. Am. Spec. Pap., pp. 79–93
Royer, D.L., Wing, S.L., Beerling, D.J., Jolley, D.W., Koch, P.L., Hickey, L.J., Berner, R.A., 2001. Paleobotanical evidence for near present-day levels of atmospheric $CO_2$ during part of the Tertiary. Science 292, 2310–2313.
Royer, D.L., Hickey, L.J., Wing, S.L., 2003. Ecological conservatism in the "living fossil" Ginkgo. Paleobiology 29, 84–104.
Royer, D.L., Berner, R.A., Park, J., 2007. Climate sensitivity constrained by $CO_2$ concentrations over the past 420 million years. Nature 446, 530–532.
Royer, D.L., Pagani, M., Beerling, D.J., 2012. Geobiological constraints on Earth system sensitivity to $CO_2$ during the cretaceous and Cenozoic. Geobiol. 10, 298–310.
Royer, D.L., Moynihan, K.M., McKee, M.L., Londoño, L., Franks, P.J., 2019. Sensitivity of a leaf gas-exchange model for estimating paleoatmospheric CO2 concentration. Clim. Past 15, 795–809.
Rubel, F., Brugger, K., Haslinger, K., Auer, I., 2017. The climate of the European Alps: Shift of very high resolution Köppen-Geiger climate zones 1800-2100. Meteorol. Z. 26, 115–125. https://doi.org/10.1127/metz/2016/0816.
Schellnhuber, H.J., Rahmstorf, S., Winkelmann, R., 2016. Why the right climate target was agreed in Paris. Nat. Clim. Chang. 6, 649–653.
Schlanser, K., Diefendorf, A.F., Greenwood, D.R., Mueller, K.E., West, C.K., Lowe, A.J., et al., 2020. On geological timescales, plant carbon isotope fractionation responds to precipitation similarly to modern plants and has a small negative correlation with $pCO_2$. Geochim. Cosmochim. $_{Acta}$ 270, 264–281.
Schubert, B.A., Jahren, A.H., 2012. The effect of atmospheric $CO_2$ concentration on carbon isotope fractionation in $C_3$ land plants. Geochim. Cosmochim. Acta 96, 29–43.
Schubert, B.A., Jahren, A.H., 2015. Global increase in plant carbon isotope fractionation following the last Glacial Maximum caused by increase in atmospheric $pCO_2$. Geology 43, 435–438.
Shaffer, G., Huber, M., Rondanelli, R., Pedersen, J.O.P., 2016. Deep time evidence for climate sensitivity increase with warming. Geophys. Res. Lett. 43, 6538–6545. https://doi.org/10.1002/2016GL069243.
Slodownik, M., Vajda, V., Steinthorsdottir, M., 2021. Fossil seed fern *Lepidopteris ottonis* from Sweden records increasing $CO_2$ concentration during the end-Triassic extinction event. Palaeogeogr. Palaeoclimatol. Palaeoecol. 564 https://doi.org/10.1016/j.palaeo.2020.110157.
Soegaard, H., Møller-Jensen, L., 2003. Towards a spatial $CO_2$ budget of a metropolitan region based on textural image classification and flux measurements. Remote Sens. Environ. 87, 283–284. https://doi.org/10.1016/S0034-4257(03)00185-8.
Soh, W.K., Wright, I.J., Bacon, K.L., Lenz, T.I., Steinthorsdottir, M., Parnell, A.C., McElwain, J.C., 2017. Palaeo leaf economics reveal a shift in ecosystem function

associated with the end-Triassic mass extinction. Nat. Plants 3, 17104. https://doi.org/10.1038/nplants.2017.104.
Sosdian, S.M., Greenop, R., Hain, M.P., Foster, G.L., Pearson, P.N., Lear, C.H., 2018. Constraining the evolution of Neogene Ocean carbonate chemistry using the boron isotope pH proxy. Earth Planet. Sci. Lett. 498, 362–376. https://doi.org/10.1016/j.epsl.2018.06.017.
South, A., 2012. rworldxtra: Country Boundaries at High Resolution. R Package Version 1.01. https://CRAN.R-project.org/package=rworldxtra.
Stein, R.A., Sheldon, N.D., Smith, S., 2019. Rapid response to anthropogenic climate change by *Thuja occidentalis*: implications for past climate reconstructions and future climate predictions. PeerJ. 7, e7378 https://doi.org/10.7717/peerj.7378.
Stein, R.A., Sheldon, N.D., Smith, S.Y., 2021. $C_3$ plant carbon isotope discrimination does not respond to $CO_2$ concentration on decadal to centennial timescales. New Phytol. 229, 2576–2585.
Steinthorsdottir, M., Vajda, V., 2015. Early Jurassic (Pliensbachian) $CO_2$ concentrations based on stomatal analysis of fossil conifer leaves from eastern Australia. Gondwana Res. 27, 932–939.
Steinthorsdottir, M., Jeram, A.J., McElwain, J.C., 2011. Extremely elevated $CO_2$ concentrations at the Triassic/Jurassic boundary. Palaeogeogr. Palaeoclimatol. Palaeoecol. 308, 418–432.
Steinthorsdottir, M., Porter, A., Holohan, A., Kunzmann, L., Collinson, M., McElwain, J.C., 2016a. Fossil plant stomata indicate decreasing atmospheric $CO_2$ prior to the Eocene-Oligocene boundary. Clim. Past 12, 439–454.
Steinthorsdottir, M., Vajda, V., Pole, M., 2016b. Global trends of $pCO_2$ across the Cretaceous-Paleogene boundary supported by the first Southern Hemisphere stomatal proxy-based $pCO_2$ reconstruction. Palaeogeogr. Palaeoclimatol. Palaeoecol. 464, 143–152.
Steinthorsdottir, M., Vajda, V., Pole, M., 2019a. Significant transient $pCO_2$ perturbation across the New Zealand Oligocene-Miocene transition recorded by fossil plants. Palaeogeogr. Palaeoclimatol. Palaeoecol. 515, 152–161.
Steinthorsdottir, M., Vajda, V., Pole, M., Holdgate, G., 2019b. Moderate levels of Eocene $pCO_2$ indicated by fossil plant stomata. Geology 47, 914–918.
Steinthorsdottir, M., Coxall, H.K., de Boer, A.M., Huber, M., Barbolini, N., et al., 2021a. The Miocene: the Future of the past. Paleoceanogr. Paleoclimatol. 36, e2020PA004037 https://doi.org/10.1029/2020PA004037.
Steinthorsdottir, M., Jardine, P.E., Rember, W.C., 2021b. Near-future $pCO_2$ during the hot mid miocene climatic optimum. Paleoceanogr. Paleoclimatol. https://doi.org/10.1029/2020PA003900.
Stoll, D.K., Guitian, J., Hernandez-Almeida, I., Mejia, L.M., Phelps, S., Polissar, P., et al., 2019. Upregulation of phytoplankton carbon concentrating mechanisms during low $CO_2$ glacial periods and implications for the phytoplankton $pCO_2$ proxy. Quat. Sci. Rev. 208, 1–20. https://doi.org/10.1016/j.quascirev.2019.01.012.
Tang, C.Q., Yang, Y., Ohsawa, M., Yi, S.-R., Momohara, A., Su, W.-H., Wang, H.-C., Zhang, Z.-Y., Peng, M.-C., Wu, Z.-L., 2012. Evidence for the persistence of wild *Ginkgo biloba* (Ginkgoaceae) populations in the Dalou Montains, southwestern China. Am. J. Bot. 99, 1408–1414.
Tomizuka, A., 2013. Why is atmospheric carbon dioxide concentration higher in the northern hemisphere? Environ. Sci. 26, 374–387.
Turnbull, J.C., Sweeney, C., Karion, A., Newberger, T., Lehman, S.J., Tans, P.P., et al., 2015. Toward quantification and source sector identification of fossil fuel $CO_2$ emissions from an urban area: results from the INFLUX experiment. J. Geophys. Res. Atmos. 120, 292–312. https://doi.org/10.1002/2014JD022555.
von der Heydt, A.S., Dijkstra, H.A., van den Wal, R.S.W., Caballero, R., Crucifix, M., Foster, G.L., et al., 2016. Lessons on climate sensitivity from past climate changes. Curr. Clim. Change Rep. 2, 148–158. https://doi.org/10.1007/s40641-016-0049-3.
Wagner, F., Below, R., DeKlerk, P., Dilcher, D.L., Joosten, H., et al., 1996. A natural experiment on plant acclimation: Lifetime stomatal frequency response of an individual tree to annual atmospheric $CO_2$ increase. Proc. Natl. Acad. Sci. U. S. A. 93, 11705–11708.
Wang, Y., Momohara, A., Wang, L., Lebreton-Anberree, J., Zhou, Z., 2015. Evolutionary history of atmospheric $CO_2$ during the late Cenozoic from fossilized *Metasequoia* needles. PLoS One 10 (7), e0130941. https://doi.org/10.1371/journal.pone.0130941.
Westerhold, T., Marwam, N., Drury, A.J., Liebrand, D., Agnini, C., et al., 2020. An astronomically dated record of Earth's climate and its predictability over the last 66 million years. Science 369, 1383–1387.
Wolfe, A.P., Reyes, A.V., Royer, D.L., Greenwood, D.R., Doria, G., Gagen, M.H., Siever, P.A., Westgate, J.A., 2017. Middle Eocene $CO_2$ and climate reconstructed from the sedimentary fill of a subarctic kimberlite maar. Geology 45, 619–622. https://doi.org/10.1130/G39002.1.
Wong, T.E., Cui, Y., Royer, D.L., et al., 2021. A tighter constraint on Earth-system sensitivity from long-term temperature and carbon-cycle observations. Nat. Commun. 12, 3173. https://doi.org/10.1038/s41467-021-23543-9.
Wood, S.N., 2017. Generalized Additive Models: An Introduction with R, 2nd edition. Chapman and Hall/CRC.
Woodward, F.I., 1987. Stomatal numbers are sensitive to increase in $CO_2$ from pre-industrial levels. Nature 327, 617–618.
Wu, J., Ding, S., Li, Q., Sun, B., Wang, Y., 2016. Reconstructing paleoatmospheric $CO_2$ levels based on fossil *Ginkgoites* from the Upper Triassic and Middle Jurassic in Northwest China. PalZ 90, 377–387. https://doi.org/10.1007/s12542-016-0300-1.
Wynn, J.G., 2003. Towards a physically based model of $CO_2$-induced stomatal frequency response. New Phytol. 157, 391–398.
Xie, S., Sun, B., Yan, D., Du, B., 2009. Altitudinal variation in *Ginkgo* leaf characters: clues to paleoelevation reconstruction. Sci. China Ser. D-Earth Sci. 52, 2040–2046. https://doi.org/10.1007/s11430-009-0157.
Xueref-Remy, I., Dieudonne, E., Vuillemin, C., Lopez, M., Lac, C., Schmidt, M., 2018. Diurnal, synoptic and seasonal variability of atmospheric $CO_2$ in the Paris megacity area. Atmos. Chem. Phys. 18, 3335–3362. https://doi.org/10.5194/acp-18-3335-2018.
Yan, W., Zhong, Y., Shangguan, Z., 2017. Contrasting responses of leaf stomatal characteristics to climate change: a considerable challenge to predict carbon and water cycles. Global Change Biol 23, 3781–3793. https://doi.org/10.1111/gcb.13654.
Yoitis, C., McElwain, J.C., 2019. A novel hypothesis for the role of photosynthetic physiology in shaping macroevolutionary patterns. Plant Physiol. https://doi.org/10.1104/pp.00749.
Yuan, W., Zheng, Y., Piao, S., Ciais, P., Lombardozzi, D., et al., 2019. Increased atmospheric vapor pressure deficit reduces global vegetation growth. Science. Advances 5, eaax1396. https://doi.org/10.1126/sciadv.aax1396.
Yue, T.X., Zhang, L.L., Zhao, M.W., Wang, Y.F., Wilson, J., 2016. Space- and ground-based $CO_2$ measurements: a review. Sci. China Earth Sci. 59, 2089–2097. https://doi.org/10.1007/s11430-015-0239-7.
Zachos, J.C., Pagani, M., Sloan, L., Thomas, E., Billups, K., 2001. Trends, rhythms and aberrations in global climate 65 Ma to present. Science 292, 686–693.
Zhang, Y.G., Pagani, M., Liu, Z., Bohaty, S., DeConto, R., 2013. A 40-million-year history of atmospheric $CO_2$. Philos. Trans. R. Soc. Lond. B 371.
Zhou, N., Wang, Y., Ya, L., Porter, A.S., Kürschner, W.M., Li, L., Lu, N., McElwain, J.C., 2020. An inter-comparison study of three stomatal-proxy methods for $CO_2$ reconstruction applied to early Jurassic Ginkgoales plants. Palaeogeogr. Palaeoclimatol. Palaeoecol. 542, 109547.
Zuur, A.F., Ieno, E.N., Walker, N.J., Saveliev, A.A., Smith, G.M., 2009. Mixed Effects Models and Extensions in Ecology with R. Springer, New York.